NATIONAL ADVISORY COMMITTEE FOR AERONAUTICS

TECHNICAL NOTE 3979

EFFECT OF BLUNTNESS ON TRANSITION FOR A CONE AND A HOLLOW CYLINDER AT MACH 3.1

By Paul F. Brinich and Norman Sands

Lewis Flight Propulsion Laboratory
Cleveland, Ohio

Washington
May 1957

NATIONAL ADVISORY COMMITTEE FOR AERONAUTICS

TECHNICAL NOTE 3979

EFFECT OF BLUNTNESS ON TRANSITION FOR A CONE AND A HOLLOW CYLINDER AT MACH 3.1

By Paul F. Brinich and Norman Sands

SUMMARY

Experimental results relating to the effect of tip bluntness and shape on transition position are presented for a 10°-included-angle cone and a hollow cylinder having its axis alined with the airstream. Both favorable and adverse effects of bluntness were found, which depended on both the shape and size of bluntness used. The largest round bluntnesses displaced transition downstream by a factor of 3 on the cylinder and 1.3 on the cone. Large sharp-cornered flat bluntnesses displaced transition upstream.

A part of the transition delay caused by bluntness is believed to be related to the unit Reynolds number reduction and Mach number reduction in the shock layer formed by the blunted leading edge. The transition delay may be further influenced by such factors as pressure gradients over the nose section, which were favorable for the cylinder and unfavorable for the cone.

Below a bluntness Reynolds number of 20,000 to 50,000, both flat and round bluntnesses had the same delaying action on transition. Above these Reynolds numbers, flat bluntness had adverse effects on transition that were believed to be caused by vortex shedding from the sharp corner of the flat bluntness.

INTRODUCTION

The size and shape of bluntness at the leading edge of an aerodynamic body have an important effect on the position of the transition from laminar to turbulent flow at supersonic speeds. In general, increasing bluntness displaces the transition point downstream (refs. 1 to 7). Reference 3 proposes an explanation for this transition delay based on the existence of a low Reynolds number layer near the surface of the body. This layer results from the leading-edge shock losses associated with bluntness and provides a low Reynolds number environment within which the

laminar boundary layer may grow. The distance to transition, assuming a constant transition Reynolds number, is therefore larger when the leading edge is blunted rather than sharp.

Numerous experiments conducted on bodies having two-dimensional boundary layers (i.e., flat plates and cylinders) exhibit the proper trend of increasing transition distance with increasing bluntness. In some of these experiments the exact value of the transition delay predicted in reference 3 was reached, whereas in others delays greater or less than the predicted values were found. Such a varied behavior suggests that the magnitude of the transition delay may be influenced by such factors as the bluntness shape or the test configuration used; possibly, factors other than the Reynolds number reduction inside the shock layer should be considered in the theory.

Despite the importance of three-dimensional bodies for high-speed missile and aircraft applications, relatively little research has been done on the effects of bluntness on such bodies. The available results (refs. 4 and 6) cover at most one or two bluntness sizes, and in general the transition delays reported are small compared with those found on the cylinder in reference 1. An exception is reference 4, where transition delays were found to approach the theoretical value due to blunting when the model temperature was reduced below the adiabatic wall temperature.

The primary objectives of this investigation were, therefore, to study the way bluntness size and shape affect transition on a conical body at equilibrium temperature, and to extend a previous cylinder bluntness investigation by considering the effects of bluntness shape and larger bluntness sizes.

APPARATUS AND PROCEDURE

Model and Instrumentation

A sketch of the 30-inch, 10°-included-angle cone used in this investigation is shown in figure 1. The cone surface was rolled, welded, and spun of 0.032-inch Inconel and polished to a surface finish of about 8 microinches rms. Cone tips made of tempered tool steel machined from solid stock were fitted to the cone body with a maximum surface irregularity of ± 0.0005 inch.

Figure 2 shows the variety of cone tip bluntnesses and shapes tested. Bluntness varied from a minimum of 0.001 inch to 0.530 inch, the latter being attained by removing the tip and plugging the hole in the end of the model. Changing the tips of the model generally involves a change of the distance from the leading edge to some fixed reference point on the cone model. In presenting the data, distances were reckoned from the leading edges of the respective tips.

Thermocouple and pressure instrumentation began 0.88 inch from the juncture of the tip and the model proper. Fifty-one copper-constantan thermocouples were arranged along the bottom generator of the model at 1/2-inch intervals, and 13 static-pressure orifices along the top at 2-inch intervals. Thermocouples were made of 0.010-inch-diameter thermocouple wire twisted together and soft-soldered into holes in the Inconel skin. The wire ends and solder were finished off flush.

The cylinder model is the same model described and tested in reference 1, except for the leading edges. These are sketched in figure 3, with bluntnesses varying from 0.0002 to 0.250 inch. Both round (semicircular cross section) and flat bluntness were used for b from 0.016 to 0.250 inch, and flat bluntness for smaller b. Stainless-steel - constantan thermocouples were spaced along the bottom generator of the model at 1/2-inch intervals.

Surface temperatures on the cone and cylinder were obtained by measuring the output of the thermocouples on a self-balancing potentiometer having a full-scale deflection of 2 millivolts. Millivolt outputs were read automatically with a digital potentiometer and recorded on punch tape. Cylinder results are believed to be in error by less than $\pm 0.5^{\circ}$ F. The cone results may have an error as large as $\pm 1.0^{\circ}$ F. Model and tunnel wall static pressures were measured on butylphthalate differential manometers to an accuracy of ± 0.002 pound per square inch. Stagnation pressures were accurate to ± 0.05 pound per square inch.

Wind Tunnel and Test Procedure

The models were tested in the NACA Lewis 1- by 1-foot variable Reynolds number wind tunnel at Mach 3.1, which is the same test facility used in references 1, 4, and 8. Test-section turbulent intensities for the present tests should be very nearly equal to those of references 1, 4, and 8 and hence make the results directly comparable. The tests were conducted at a stagnation temperature of $75^{\circ} \pm 2^{\circ}$ F and in the stagnation-pressure range of 7 to 50 pounds per square inch absolute, giving a unit Reynolds number range of 1×10^5 to 6.7×10^5 per inch.

Transition positions were obtained from the location of the peak temperature between the laminar and turbulent regions. These locations could be verified by instantaneous schlieren photographs within a range of ± 1 inch. Between five and ten schlieren photographs were used in each comparison.

RESULTS

Recovery-Factor and Pressure Distributions on Cone

Of all the cone tips shown in figure 2, the flat (A) and round (C) bluntnesses represent two extremes insofar as their effect on transition is concerned. Hence, the detailed recovery factor and pressure distributions will be given for these tip geometries only. All temperature distributions using other cone tips may be assumed to fall somewhere between these two; or, if any relevant differences exist, these will be mentioned specifically.

Recovery-factor distribution η', based on inviscid sharp-cone surface conditions ($M_s = 3.0$), is plotted against x in figures 4(a) and (b) for the flat and round bluntnesses, respectively, for a typical unit Reynolds number u_∞/ν_∞ of 3.5×10^5 per inch. For convenience, the distance to transition was measured parallel to the cone centerline rather than along the model surface; this introduces a slight but negligible error in the distance to transition. Temperature-peak locations between the laminar and turbulent regions closely approximate the mean transition location obtained from schlieren photographs (indicated by downward-pointing arrows in fig. 4). Since the temperature distributions were quite precise and more convenient to work with, they were used to determine the transition position. The distance to transition was measured from the actual blunted tip to the temperature peak.

Variations in cone bluntness from 0.001 to 0.006 inch produced no variation in the distance to transition nor in the temperature distribution. Increases in flat bluntness to 0.063 and 0.125 inch resulted in respective downstream displacements of the transition point to $x = 11.5$ and 14 inches compared with an initial value for x of 10.3 inches. A further increase in flat bluntness to 0.250 inch displaced transition upstream to $x = 8$ inches, this upstream trend continuing with increasing bluntness.

Figure 4(b) shows that increasing the round bluntness to 0.250 inch displaced transition from its original position at $x = 10.3$ inches to $x = 12.5$ inches. Transition then remained approximately fixed as the bluntness was increased to the maximum tested value of 0.530 inch. Such increases in transition distance are slight compared with those reported for the cylinder in reference 1 or the theoretical predictions of reference 3. The slight superiority of the 0.125-inch flat over the 0.125-inch round tip may be due to the greater thickness of the shock layer produced by the flat bluntness. In the discussion of figure 4 the sharp-cone tips ($b = 0.001$ and 0.006 in.) are compared with flat and round bluntness interchangeably. This is justified because of the insignificant effect of bluntness shape when the bluntness is small.

Figure 4 also reveals increases in the laminar recovery factor as the leading-edge bluntness is increased. These apparent increases were caused by the Mach number reduction inside the shock layer and were also observed in reference 1, where bluntness effects on a hollow cylinder were investigated. These increases in recovery factor with increasing bluntness are a direct result of using the inviscid sharp-cone surface Mach number M_s rather than the appropriate shock-layer Mach number M_δ at the boundary-layer outer edge for computing the recovery factor. The free-stream recovery factor η' is given by the following equation when the outer-edge Mach number M_δ, the stream Mach number M_s, and the true recovery factor η are known:

$$\eta' = \frac{M_s^2 + M_\delta^2 \left[\eta\left(1 + 0.2\, M_s^2\right) - 1\right]}{M_s^2\left(1 + 0.2\, M_\delta^2\right)} \tag{1}$$

This equation may be derived from the definitions for η and η' given in appendix A by equating the wall temperature T_w.

The maximum value of η' will be reached when M_δ is a minimum; that is, when the entire boundary layer is within the lowest Mach number region of the shock layer. The minimum value of M_δ is found from figure 1 of reference 3 to be about 2.2 for the present cone at a flight Mach number M_∞ of 3.1. Using these conditions together with the fact that the true laminar recovery factor for the sharp cone is 0.845 and the inviscid surface Mach number $M_s = 3.0$, the maximum laminar recovery factor η' is found from equation (1) to be 0.881. The maximum measured recovery factor for the laminar region of figures 4(a) and (b) is about 0.877. This is rather close agreement between experiment and theory, since the temperature error involved is less than 2° F. The existence of the shock layer on the cone is thus established as it was in the blunt-cylinder studies of reference 1. The increase in turbulent recovery factor for the largest bluntness in figure 4(b) is evidence that for these bluntnesses the shock layer extends over the turbulent part of the body as well as the laminar.

For convenience, equation (1) is plotted in figure 5 for a range of stream Mach numbers from 1 to 5. Also shown are limiting lines which determine the maximum recovery factor attainable throughout the Mach number range because of a shock layer as analyzed in reference 3 and the minimum line at $\eta = 0.845$ which was obtained with the sharp-tipped cone. Values below this minimum might be obtained in regions where the flow expands below the ambient pressure, and values above the maximum are possible if the flow were compressed sufficiently above the ambient pressure. Figure 5 may also be used to determine the outer-edge Mach number M_δ when the bluntness is less than enough to immerse the entire laminar

boundary layer inside the lowest Mach number portion of the shock layer, provided that η' is known, the boundary layer is fully laminar, and $\eta = 0.845$.

Pressure distributions along the top of the model are shown in figures 6(a) and (b) for the flat and round bluntnesses, respectively, at $u_\infty/\nu_\infty = 3.5\times10^5$ per inch. The curves faired through the experimental points for the various bluntnesses show pressure variations along the surface, some of which are common to all the bluntnesses and others which are peculiar to each. Since the experimental points are all plotted from the actual model tip rather than as a function of position in the tunnel, most of the pressure variations downstream of $x \sim 8$ inches are caused by the tunnel flow. One exception is the small pressure rise for the largest bluntnesses at the most downstream location where the reflected shock from the blunt leading edge impinges.

The pressure variations upstream of about 8 inches, however, are due to the various degrees of bluntness used. In this region the pressure gradient is definitely adverse for the three largest bluntnesses. The primary effect of bluntness shape was a steepening of the pressure gradient near the nose when the flat bluntness was used, compared with that obtained with the round bluntness. The pressure distributions of figure 6 are quite independent of the stream Reynolds number.

Effect of Unit Reynolds Number and Bluntness on Transition Location on Cone

Flat bluntness. - The effect of unit Reynolds number and size of flat bluntness is illustrated in figure 7(a). The distance to transition for the sharp-tip (0.001 to 0.006 in.) cones is indicated by a solid line, which may be represented by a power-type relation as in reference 8:

$$x_t = 46{,}500(u_\infty/\nu_\infty)^{-0.66} \qquad (2)$$

or in terms of the transition Reynolds number Re_t:

$$Re_t = 46{,}500(u_\infty/\nu_\infty)^{0.34}$$

where x_t is the distance to transition in inches and u_∞/ν_∞ the Reynolds number per inch.

The important features of figure 7(a) are the increases in distance to transition using small sharp-cornered flat bluntnesses and the generally decreased distance to transition for larger bluntnesses, particularly at large u_∞/ν_∞. The 0.063-inch bluntness is slightly beneficial

at all u_∞/ν_∞. The 0.125-inch tip, however, moved transition ahead of the position for the sharp tip at $u_\infty/\nu_\infty > 5.5\times10^5$ per inch and downstream of the 0.063 tip position for $u_\infty/\nu_\infty < 5.25\times10^5$ per inch. As the bluntness is increased further, the same trends can be detected until finally the 0.530 tip is worse than the sharp tip for all u_∞/ν_∞.

To determine the effect of the sharp corner on the flat blunted tips, the corner of the 0.375 tip was rounded to 0.063-inch radius as sketched in figure 2 (config. B). Transition was then found at the same position as for the sharp tip or somewhat downstream. The resulting pressure distribution was the same as that obtained with the flat tip. Hence, it is believed that the adverse behavior of the sharp-cornered flat bluntness as compared with the slightly rounded flat bluntness is primarily a vortex-shedding effect associated with the sharp corner.

Round bluntness. - The distances to transition for the various round bluntnesses sketched in figure 2 (config. C) are compared in figure 7(b) with the sharp-cone transition distance as a function of the unit Reynolds number. All the hemispherical tips proved to be only slightly superior to the sharp tip throughout the Reynolds number range, practically independently of the bluntness size. It will also be noted in figure 7(b) (and fig. 7(a) for the smaller bluntnesses) that a transition plateau exists at about $x_t = 16$ inches for the blunted cone at unit Reynolds numbers u_∞/ν_∞ between 1.8×10^5 and 2.7×10^5 per inch. At this position an adverse pressure gradient caused by the tunnel flow was observed in figure 6. This gradient was present at all Reynolds numbers and for all bluntnesses, including the sharp cone. Apparently, the transition position is more sensitive to the existence of small pressure gradients after transition has been delayed by blunting than it is on the sharp cone.

An interesting phenomenon was observed when a sharp 3-inch needle was extended forward from the stagnation point of the 0.530-inch round bluntness (tip D, fig. 2). Turbulent flow was immediately established at the round tip for all Reynolds numbers. Schlieren photographs indicated that unsteady-flow separation occurred on the needle, and recovery factors on the forward part of the model were less than the laminar value.

Conical bluntness. - The effect of several conical tip geometries (configs. E, F, and G, fig. 2) on the distance to transition is presented in figure 7(c) and compared with the results for the sharp tips. All of the conical tips were somewhat inferior to the sharp ones except the 0.250 tip with the 60° included angle (tip E) in the range of unit Reynolds numbers from 0.9×10^5 to about 2×10^5 per inch. Decreasing the 0.530-inch cone tip included angle from 60° to 30° (config. G) produced a slight downstream movement of transition in the high unit Reynolds number range.

Again, to determine whether rounding of the shoulder improved the transition characteristics, an ogive tip (config. H) having a 60° included tip angle and the same length as configuration E was tested. This tip showed transition characteristics almost identical to the sharp tip, again indicating some destabilizing effect due to the sharp corner turn for the conical bluntnesses. Recovery factors in the laminar region were very close to the true laminar value, indicating an outer-edge Mach number for the boundary layer of 2.91 to 2.94 for the 60° tip angle, which is to be compared with a theoretical value of about 2.9 computed from oblique shock losses for a 60°-included-angle tip with subsequent reexpansion.

Miscellaneous bluntnesses. - In order to extend the present investigation and possibly obtain additional insight into the transition problem, several other elementary shapes were also tested. These included two sharp tips having 10° angles, one being 0.13 inch undersize at the juncture of the tip and the cone body proper and the other 0.13 inch oversize (configs. I and J, fig. 2). Figure 7(d) shows that the performance of the oversized tip is considerably better than that of the undersized, the distance to transition being measured from the forward extremity of the tip. The undersized tip exhibited unsteady-separation phenomena similar to those mentioned for the hemispherical tip with needle.

Two other configurations shown in figure 7(d) are 0.530-inch-diameter straight extensions (configs. K and L, fig. 2) having flat and round tips. Again the round tip gave superior performance, equalling the standard sharp tip at low unit Reynolds numbers. These findings suggest that the shape of the bluntness retains its relative importance on three-dimensional body shapes other than cones.

Recovery-Factor and Pressure Distributions on Cylinder

The effect of flat bluntness on transition for a hollow cylinder is reported in reference 1. After the present cone-bluntness study was completed, it became evident that the original cylinder study should be extended to include larger bluntnesses than previously tested and also to study the effect of round bluntness. In repeating certain of the earlier cylinder work it was found that transition occurred about 1/2 inch downstream of the positions given in reference 1 for the 5° leading edge, particularly in the high unit Reynolds number range and for small bluntnesses. This observation indicated that some structural instability may have existed in the 5° leading edge used in reference 1 compared with the present 15° edge. Transition locations for the present leading edge compare exactly with the 30° leading edge tested in reference 1. It should therefore experience negligible distortion or vibration.

Recovery-factor distributions η' against x are indicated for the cylinder in figure 8 for a typical unit Reynolds number of 3.5×10^5 per inch and bluntnesses ranging from 0.0002 to 0.250 inch. Transition positions as indicated by temperature-peak locations move downstream substantial amounts as the bluntness is increased, except for the 0.096- and 0.250-inch sharp-cornered flat bluntness, where the transition movement is reversed. These two latter leading edges illustrate a behavior similar to that observed with the larger flat bluntnesses on the cone. Also, it is important to note that the temperature peaks for the 0.096- and 0.250-inch round bluntness at $x = 14.8$ and 13 inches were caused by the blunt-leading-edge shock reflection as well as by transition, and that the transition delay due to bluntness was definitely hampered by the shock reflection.

A gradual increase in the laminar recovery factor from 0.855 to 0.880 as the bluntness is increased from 0.0002 to 0.0114 inch is apparent. The smaller increase from 0.880 to 0.885 as the bluntness is increased further to 0.250-inch round indicates an asymptotic increase to the maximum value possible in the shock layer. The maximum theoretical value for η' is seen to be 0.877 from figure 5. Figure 5 is based on a measured laminar recovery factor of 0.845 obtained on the sharp cone. If the measured recovery factor ($\eta = 0.855$) found for the sharp leading edge in figure 8 is used to evaluate equation (1), then a theoretical maximum value for η' of 0.888 will be found, which agrees very well with the measured asymptotic value.

Also apparent in figure 8 is an abrupt increase in the turbulent recovery factor for $x > 18$ inches from 0.883 for bluntnesses $b \leq 0.024$ inch to a value of 0.896 for $b = 0.051$ inch. The 0.096- and 0.250-inch leading edges reach an asymptotic value of about 0.915. The maximum value possible considering the Mach number reduction in the shock layer gives $\eta' = 0.911$. This value is obtained from equation (1), but using a turbulent recovery factor η of 0.883 (taken from fig. 8, $b = 0.0002$ in.). This close agreement between experiment and theory shows that the integrity of the shock layer can be maintained across the transitional and turbulent regions as well as over the laminar boundary layer. The much larger bluntnesses required to achieve the maximum theoretical value for η' result from the abrupt increase in thickness of the transitional and turbulent boundary layers as compared with the preceding laminar layer.

Cylinder pressure distributions corresponding to the recovery-factor plots are shown in figure 9 for the blunted cylinder at $u_\infty/\nu_\infty = 3.5\times10^5$ per inch. The pressure in general follows a rising trend going downstream with small vertical oscillations. Exceptions to this behavior occur with the bluntest leading edges ($b = 0.096$ and 0.250 in.), where a favorable pressure gradient near the nose and a sharp pressure rise about 14 inches downstream appear. This pressure rise is due to the strong reflected leading-edge shock and interferes with the downstream movement of

transition as noted in figure 8 for the larger round bluntnesses. The favorable pressure gradient near the nose for the 0.096- and 0.250-inch bluntnesses is to be contrasted with the adverse gradients observed near the blunted tip of the cone. These differences in pressure gradient might account for the smaller benefits realized from bluntness on the cone compared with the cylinder. In contrast with the recovery-factor plots, there is very little effect of bluntness shape on pressure distribution. The pressure gradients near the leading edge are more favorable for the large flat bluntnesses than for the round, and also the shock interaction due to the reflection of the leading-edge shock is more severe for the flat than for the round bluntnesses.

Effect of Unit Reynolds Number and Bluntness on Transition Location on Cylinder

Figure 10 shows that, for bluntnesses from 0.0002 to about 0.0079 inch, the distance to transition on a cylinder in general increases with increasing bluntness. The sharp leading edge is represented by the 0.0002-inch bluntness data, which fall along approximately a straight line having the equation

$$x_t = 36{,}330(u/\nu)^{-0.7} \tag{3}$$

or

$$Re_t = 36{,}330(u/\nu)^{0.3}$$

In the bluntness range from 0.0079 to 0.024 inch, there is a negligible movement of the transition point. Within this region the maximum ratio of the distance to transition with and without bluntness is about 2.1, which is close to the value predicted in reference 3. This prediction is based on the assumption that the transition delay results from the unit Reynolds number reduction in the shock layer, which is the inverse ratio of 2.1. In reference 1 a similar behavior was observed for bluntnesses ranging from 0.008 to 0.043 inch, the latter being the maximum size tested.

All the cylinder results in figure 10 described so far were obtained only with flat bluntnesses, with the exception of the 0.016 and 0.024 inch, which were obtained with round as well as flat. These round and flat bluntnesses gave identical transition positions, and it must be conjectured that the same result would be obtained if round bluntness had been used for sizes smaller than 0.016 inch also.

Beginning with a bluntness of 0.051 inch, the effect of shape as well as size becomes important. Increasing the round bluntness to 0.096

and 0.250 inch displaces the transition point farther downstream, whereas the corresponding sharp-cornered flat bluntnesses move it upstream, particularly in the high unit Reynolds number range. The maximum downstream movement of transition using the larger round bluntnesses is limited by the strong leading-edge shock, which is reflected back on the model about 14 inches from the leading edge.

DISCUSSION

The results presented thus far show rather large variations in the transition delay obtained on a blunted cone and cylinder, making a straightforward correlation of the results difficult. Before discussing any particular correlation between the cone and cylinder results, certain points of similarity between the two should be recalled: (1) the universally favorable effect of round bluntness regardless of size, (2) the decreased or unfavorable effect of sharp-cornered flat bluntnesses above a certain size on transition, and (3) the existence of the shock layer on the cone and cylinder of sufficient thickness in many instances to completely immerse the laminar boundary layer within the low Reynolds number part of the shock layer. The primary question now to be resolved is why the transition delays observed on the blunted cone are so much smaller than those found for the cylinder.

Parameters that summarize the cone and cylinder results and partially correlate them are given by the equation

$$\frac{x_{t,b}}{x_{t,0}} = F\left(\frac{u_\infty b}{\nu_\infty}\right) = F(Re_b) \qquad (4)$$

where $x_{t,b}/x_{t,0}$ is the ratio of the distance to transition blunted to that unblunted, and $u_\infty b/\nu_\infty$ is the bluntness Reynolds number based on free-stream flow conditions. A similar correlation, but with $x_{t,b}/x_{t,0}$ replaced by the transition Reynolds number $u_\infty x_{t,b}/\nu_\infty$ is used in reference 5. Because of the strong dependence of transition on the stream unit Reynolds number, the transition-distance ratio is considered more desirable.

The cone results using the parameters in equation (4) for the flat and round bluntnesses are plotted in figures 11(a) and (b), respectively, and the corresponding plots for the cylinder are shown in figure 11(c). In general, the transition-distance ratio for the cylinder increases with increasing bluntness Reynolds number until a value of $x_{t,b}/x_{t,0}$ of nearly 3 is reached for the largest round bluntness tested (fig. 11(c)). Exceptions to this general behavior are apparent. For one thing the transition-distance ratio decreases with increasing Re_b over a

considerable Reynolds number range for the 0.096- and 0.250-inch flat bluntnesses. In the latter case the transition-distance ratio drops to 0.65 at the maximum bluntness Reynolds number. This reduced effectiveness of flat bluntness becomes apparent first at $Re_b \sim 20,000$ on the cylinder.

At high values of Re_b a similar trend of decreasing transition-distance ratio for increasing bluntness Reynolds number is apparent for cylinder bluntnesses between 0.0031 and 0.051 inch. This diminishing effectiveness of bluntness when transition is near the leading edge may be caused by local static-pressure variations that give transition a preferred position distinct from that dictated by conditions within the shock layer. This effect of local pressure variation on transition position is difficult to prove, since transition by itself sometimes produces its own local pressure rise, which is of about the same magnitude as the local pressure variations due to the tunnel flow. It is not unreasonable to expect that, if the model static-pressure distribution due to the tunnel flow were perfectly uniform, the wiggles in most of the curves shown in figure 11(c) would disappear.

The static-pressure rise produced by the reflected shock from the larger round blunted leading edges was seen in figures 8 to 10 to retard or halt the downstream progress of the transition point. This effect is also apparent in figure 11(c), where the level of the bluntness Reynolds number curves (in particular that portion of the curves having a positive slope) is seen to rise as the bluntness is increased from 0.051 to 0.096 and to 0.250 inch. The variation of $x_{t,b}/x_{t,0}$ in all but the high Reynolds number range for these bluntnesses reflects changes in $x_{t,0}$ rather than in $x_{t,b}$, which was fixed more or less by the reflection of the strong leading-edge shock.

The bluntness Reynolds number required for the outer edge of the laminar boundary layer to be inside the low-velocity part of the shock layer up to the transition point can be evaluated for the cylinder by use of equations (11) and (12) of reference 3 and equation (3) of the present report. This calculation gives bluntness Reynolds numbers from 1300 to 1700 for the range of unit Reynolds numbers tested. These values are close to the minimum experimental values of Re_b (~2000, fig. 11(c)), which give transition delays near the theoretical value of 2.17 predicted in reference 3.

In connection with the theoretical transition-distance ratio of 2.17 given by reference 3 for the present cylinder and cone test conditions, the following remarks are pertinent. The transition delays predicted in reference 3 were based on the assumption that the transition Reynolds number is unaffected by blunting, whereas it is known from experiment that both the Mach and unit Reynolds numbers can influence the

transition Reynolds number. However, for the present tests the increase in Re_t caused by the reduction in boundary-layer outer-edge Mach number is cancelled almost exactly by the decrease in Re_t resulting from the decreased outer-edge unit Reynolds number.

This cancellation of the two opposing effects can be illustrated with the aid of some flat-plate results of reference 9, reproduced in figure 12. (These results are the average transition Reynolds numbers obtained by various techniques.) Following the arrow in figure 12 shows that Re_t increases from 2.2×10^6 to 3.0×10^6 at a unit Reynolds number of 4×10^5 per inch when the Mach number is reduced from 3.1 to 2.3. But halving the unit Reynolds number at M_∞ of 2.3 (as would occur in the shock layer) from 4×10^5 to 2×10^5 per inch reduces Re_t almost to its original value. (The same cancellation was observed in unpublished data obtained on a cone at this laboratory.) It thus appears that the transition delay suggested in reference 3 agrees well with the delay obtained by a consideration of both the Mach and unit Reynolds number reduction in the present instance. In general, this agreement may not be true at other Mach numbers, but as yet insufficient data are available to make reliable estimates of the magnitudes of the combined effects.

The plots of Re_b against $x_{t,b}/x_{t,0}$ for the flat and round blunted cones (figs. 11(a) and (b)) show transition-distance ratios considerably smaller than obtained on the cylinder. The maximum ratio $x_{t,b}/x_{t,0} \sim 1.3$ obtained with the blunted cone is to be compared with a ratio of 2 or 3 obtained on the blunted cylinder. Again, the bluntness Reynolds number required in order that the laminar boundary layer be within the low-velocity part of the shock layer may be computed from equations (11) and (13) of reference 3 and equation (2) of the present report. For the test Reynolds number range used herein, the value of Re_b required varied from 20,000 to 33,000 on the flat blunted cone. Comparison of these results with the experimental values of Re_b at which the maximum transition delay is first obtained in figure 11(a) shows fair agreement.

Comparison of figures 11(a) and (b) shows that the results for the flat blunted cone follow the same trends as the round up to $Re_b \sim 50{,}000$. Beyond this point bluntness has an adverse effect on transition, and ratios as low as 0.23 are reached at the highest Reynolds numbers.

Figure 11(d) is a composite of figures 11(a) to (c)in which those points for the cylinder which were influenced by the leading-edge reflected shock have been deleted. The wiggles in figures 11(a) to (c), which were considered to be small local pressure-gradient effects, have been removed by visually passing a mean line through the various points.

The theoretical value for $x_{t,b}/x_{t,0}$ from reference 3, which considers only the Reynolds number reduction in the shock layer, falls close to the cylinder points in the range of Re_b from 3000 to 20,000. Transition delays greater than the theoretical value were obtained with the 0.096- and 0.250-inch round bluntnesses, and may be attributed to the favorable pressure gradients over the forward portion of the model (see fig. 9). These two leading edges also gave shock layers that were preserved in the turbulent region, as indicated by recovery factors η' close to the maximum possible for a turbulent boundary layer in a shock layer. It is interesting to note that the 0.096- and 0.250-inch flat bluntnesses with sharp corners also had favorable pressure gradients near the leading edge and shock layers that were preserved through the turbulent region, but nevertheless had adverse effects on the transition delay. This behavior suggests again that the adverse effect of sharp-cornered flat bluntness is a phenomenon unrelated to the pressure gradient and the formation of a shock layer. The close proximity of the flat-bluntness portion of the curves for the cone and the cylinder toward the upper left of figure 11(d) indicates a very close correlation of the adverse flat-bluntness effects on a cone and cylinder when the bluntness Reynolds number Re_b is used as a correlating parameter. The fact that a much larger value of Re_b is required to obtain any transition delay on the cone than on the cylinder (8000 for the cone compared with 80 for the cylinder) is to be expected, since the shock layer on the cone is produced near a point source, whereas that for the cylinder is produced by an annular bluntness.

Although figure 11(d) seems to correlate the adverse effect of flat bluntness on the cone and cylinder (which is due to the sharp corner on the bluntness), it does not correlate the beneficial effect of blunting on transition obtained with the rounded bluntnesses. This happens because the parameter Re_b does not take into account the thinning of the shock layer on the cone. If this thinning is accounted for, a new parameter called the adjusted bluntness Reynolds number $Re_{b,a}$, derived in appendix B, is defined which takes the place of Re_b. In this development, the shock-layer height at the transition point is considered of particular significance. Also taken into account are bluntness differences caused by bluntness shape (round and flat) and differences in shock-layer area between a cone and a cylinder as given in reference 3. Figures 13(a) and (b) present the results for the flat and round blunted cones in terms of the parameters $Re_{b,a}$ against $x_{t,b}/x_{t,0}$. These figures show the same trends as figures 11(a) and (b) but with different values in the ordinate.

The results of figures 13(a) and (b) are compared with the blunt-cylinder results in figure 13(c). The various data points are represented by curves that neglect the irregularities caused by tunnel pressure gradients and the points influenced by the strong leading-edge shock

reflections. The cone and cylinder results are now seen to agree for Reynolds numbers up to $Re_{b,a} \sim 300$, indicating that in this range the shock-layer height at the transition point seems to correlate the favorable effect of blunting on both the cone and the cylinder. For $Re_{b,a} > 300$, there is little change in the transition-distance ratio for a round blunted cone; and at $Re_{b,a} > 1000$, flat bluntness begins to have an adverse effect on transition.

A question raised by figure 13(c) is, Why does cone bluntness have the same effect as cylinder bluntness only up to the point $Re_{b,a} = 300$? The answer to this may be that for $Re_{b,a} < 300$ the adverse pressure gradient associated with the blunted cone (figs. 6(a) and (b)) occurs sufficiently far forward to be in the stable part of the laminar boundary layer, perhaps below the minimum critical Reynolds number. (The Reynolds number $u_\infty x/\nu_\infty$ at the bluntness shoulder corresponding to $Re_{b,a} \sim 300$ is about 30,000.) Conversely, when $Re_{b,a} > 300$, the adverse pressure gradient occurs farther downstream, possibly in the unstable part of the laminar boundary layer, thus promoting earlier transition.

To summarize figures 11(d) and 13(c), the effect of blunting on a cylinder (or flat plate) is to delay transition for either round or flat bluntness as long as $Re_{b,a}$ or Re_b is less than about 20,000. Above 20,000, round bluntnesses give further beneficial effects and sharp-cornered flat bluntnesses give adverse effects. The effect of bluntness on a cone consists of a favorable influence due to the shock layer and an adverse influence probably brought about by the location of adverse pressure gradients near the nose. Above $Re_{b,a} \sim 500$ or $Re_b \sim 50{,}000$, the transition point for the round blunted cone at a given value of u_∞/ν_∞ becomes virtually fixed, indicating some sort of balance between the two opposing effects.

CONCLUDING REMARKS

Transition delays obtained with bluntness on a cylinder (or flat plate) are much larger than those found on a cone. Transition delays as high as a factor of 3 were obtained on a cylinder compared with a maximum of 1.3 for the cone. Both of these values are to be compared with the theoretical value of 2.17 of reference 3, which is based on the Reynolds number reduction in the shock layer.

The effect of bluntness on the pressure distribution was to produce a favorable pressure gradient over the forward part of the cylinder and an adverse gradient over the corresponding part of the cone. The adverse gradient for the cone has been interpreted as a destabilizing factor that does not permit the full benefit of the shock layer to be realized. It

has been suggested that the transition delays in excess of the value predicted in reference 3 may be caused by the favorable pressure distribution observed with the largest bluntnesses over the forward part of the cylinder.

The effect of bluntness shape - that is, flat or rounded - on transition delay was insignificant below a bluntness Reynolds number of 20,000 for the cylinder and 50,000 for the cone. Above these Reynolds numbers the flat bluntness had a strong detrimental effect on transition. This effect is believed to be due to a vortex shedding off the sharp corners, which in turn introduces disturbances into the laminar boundary layer. Very slight rounding of the sharp corners increased the distance to transition greatly. A similar phenomenon was also observed when the bluntness was conical in form rather than flat.

The shock layer was present over both the blunted cone and cylinder. When the bluntness was sufficiently large, surface recovery temperatures corresponding to the maximum Mach number reduction in the shock layer predicted in reference 3 were obtained in the laminar and turbulent regions. These recovery factors were obtained with both flat and round bluntnesses.

The destabilizing effect of sharp-cornered flat bluntness on the cone and cylinder can be correlated using the bluntness Reynolds number as a parameter. The favorable effect of the shock layer in delaying transition on the cone and cylinder can be partly correlated by using an adjusted bluntness Reynolds number that is proportional to the Reynolds number based on shock-layer height at the transition point. This latter correlation is valid up to an adjusted Reynolds number of 300.

Lewis Flight Propulsion Laboratory
National Advisory Committee for Aeronautics
Cleveland, Ohio, February 12, 1957

APPENDIX A

SYMBOLS

A_n	shock-layer height as defined in ref. 3
A_{SB}	bluntness area as defined in ref. 3
b	bluntness (figs. 2 and 3)
C_p	pressure coefficient $(p - p_\infty)/q_\infty$
F	arbitrary function
M	Mach number
p	static pressure
q	dynamic pressure
Re	Reynolds number
Re_b	bluntness Reynolds number defined by eq. (4)
$Re_{b,a}$	adjusted bluntness Reynolds number defined by eqs. (B6) and (B7)
r	body radius
T	absolute temperature
u	velocity
u/ν	unit Reynolds number
x	distance along model parallel to centerline from physical tip of model
y_b	bluntness diameter at sonic point
y_n	shock-layer height as defined in appendix B
η	recovery factor based on conditions at edge of boundary layer, $\eta = \frac{T_w - T_\delta}{T_0 - T_\delta}$

η' recovery factor based on conditions outside shock layer; $\eta'(\text{cone}) = \frac{T_w - T_s}{T_0 - T_s}$; $\eta'(\text{cylinder}) = \frac{T_w - T_\infty}{T_0 - T_\infty}$

ν kinematic viscosity

Subscripts:

b conditions for blunted model

s inviscid sharp-cone surface conditions

t conditions at transition point

w wall values

δ conditions at edge of boundary layer

0 stagnation conditions or zero bluntness

1,2,3,4 subscripts denoting different functions

∞ free-stream values

APPENDIX B

DERIVATION OF ADJUSTED CONE BLUNTNESS REYNOLDS NUMBER

It is desired to compute the cone bluntness Reynolds number in order to account for the thinning of the shock layer. To do so, it will be assumed that the fundamental parameter which expresses the stabilizing effect of bluntness on a cone or cylinder is

$$\frac{x_{t,b}}{x_{t,0}} = F\left(\frac{u_\infty y_{n,t}}{\nu_\infty}\right) \tag{B1}$$

where $y_{n,t}$ is the height of the shock-produced layer at the transition point.

For a cylinder, according to reference 3,

$$y_{n,t} = \frac{A_n}{A_{SB}} \frac{2\pi r y_b/2}{2\pi r} \tag{B2}$$

where the area ratio A_n/A_{SB} is given in figure 3 of reference 3 as 2.95 for a flat plate (or cylinder) and 2.45 for a 10°-included-angle cone at Mach 3.1. The quantity y_b is the bluntness diameter at the sonic point on the bluntness (ref. 3). When the bluntness is flat, $y_b = b$; when it is round, y_b is 0.822 b for the cylinder and 0.647 b for the cone (for $M_\infty = 3.1$). The height of the shock layer $y_{n,t}$ is defined, as in reference 3, to be the distance above the surface of that streamline which passes through the sonic point of the detached shock. For the cylinder, equation (B1) becomes

$$\frac{x_{t,b}}{x_{t,0}} = F_1\left(\frac{1.475\ u_\infty y_b}{\nu_\infty}\right) \tag{B3}$$

The shock-layer height at transition for the cone is given by

$$y_{n,t} = \frac{A_n}{A_{SB}} \frac{\pi(y_b/2)^2}{2\pi r_t} \tag{B4}$$

where r_t is the cone radius at the transition point and is given by

$$r_t = \frac{b}{2} + x_{t,b} \tan 5^\circ$$

where $x_{t,b}$ is the distance to transition. Equation (B1) for the cone becomes

$$\frac{x_{t,b}}{x_{t,0}} = F_2\left(\frac{1.225\ y_b}{2b + 0.349x_{t,b}}\ \frac{u_\infty y_b}{\nu_\infty}\right) \tag{B5}$$

Dividing the terms in the parentheses of equations (B3) and (B5) by 1.475 gives for the cylinder

$$\frac{x_{t,b}}{x_{t,0}} = F_3\left(\frac{u_\infty y_b}{\nu_\infty}\right)$$

$$= F_3(Re_{b,a})$$

$$= F_3(Re_b) \tag{B6}$$

and for the cone

$$\frac{x_{t,b}}{x_{t,0}} = F_4\left(\frac{0.83\ y_b}{2b + 0.349x_{t,b}}\ \frac{u_\infty y_b}{\nu_\infty}\right)$$

$$= F_4(Re_{b,a}) \tag{B7}$$

Equations (B6) and (B7) define the parameters plotted in figure 13.

REFERENCES

1. Brinich, Paul F.: Effect of Leading-Edge Geometry on Boundary-Layer Transition at Mach 3.1. NACA TN 3659, 1956.

2. Brinich, Paul F., and Diaconis, Nick S.: Boundary-Layer Development and Skin Friction at Mach 3.05. NACA TN 2742, 1952.

3. Moeckel, W. E.: Some Effects of Bluntness on Boundary-Layer Transition and Heat Transfer at Supersonic Speeds. NACA TN 3653, 1956.

4. Diaconis, N. S., Jack, John R., and Wisniewski, Richard J.: Boundary-Layer Transition at Mach Number 3.12 as Affected by Cooling and Nose Blunting. NACA TN 3928, 1957.

5. Bertram, Mitchel H.: Exploratory Investigation of Boundary-Layer Transition on a Hollow Cylinder at a Mach Number of 6.9. NACA TN 3546, 1956.

6. Witt, W. R., Jr.: Free Flight Boundary Layer Transition Studies on Cones. Fourth Midwestern Conf. on Fluid Mech., Purdue Univ. Eng. Bull., 1955, pp. 297-313.

7. Dunning, Robert W., and Ulmann, Edward F.: Effects of Sweep and Angle of Attack on Boundary-Layer Transition on Wings at Mach Number 4.04. NACA TN 3473, 1955.

8. Brinich, Paul F.: A Study of Boundary-Layer Transition and Surface Temperature Distributions at Mach 3.12. NACA TN 3509, 1955.

9. Coles, Donald: Measurements in the Boundary Layer on a Smooth Flat Plate in Supersonic Flow. III - Measurements in a Flat-Plate Boundary Layer at the Jet Propulsion Laboratory. Rep. No. 20-71, Jet Prop. Lab., C.I.T., June 1, 1953. (Contract No. DA-04-495-Ord 18, Dept. Army, Ord. Corps.)

10. Anon.: Tables of Supersonic Flow Around Cones. Tech. Rep. No. 1, Dept. Elec. Eng., M.I.T., 1947.

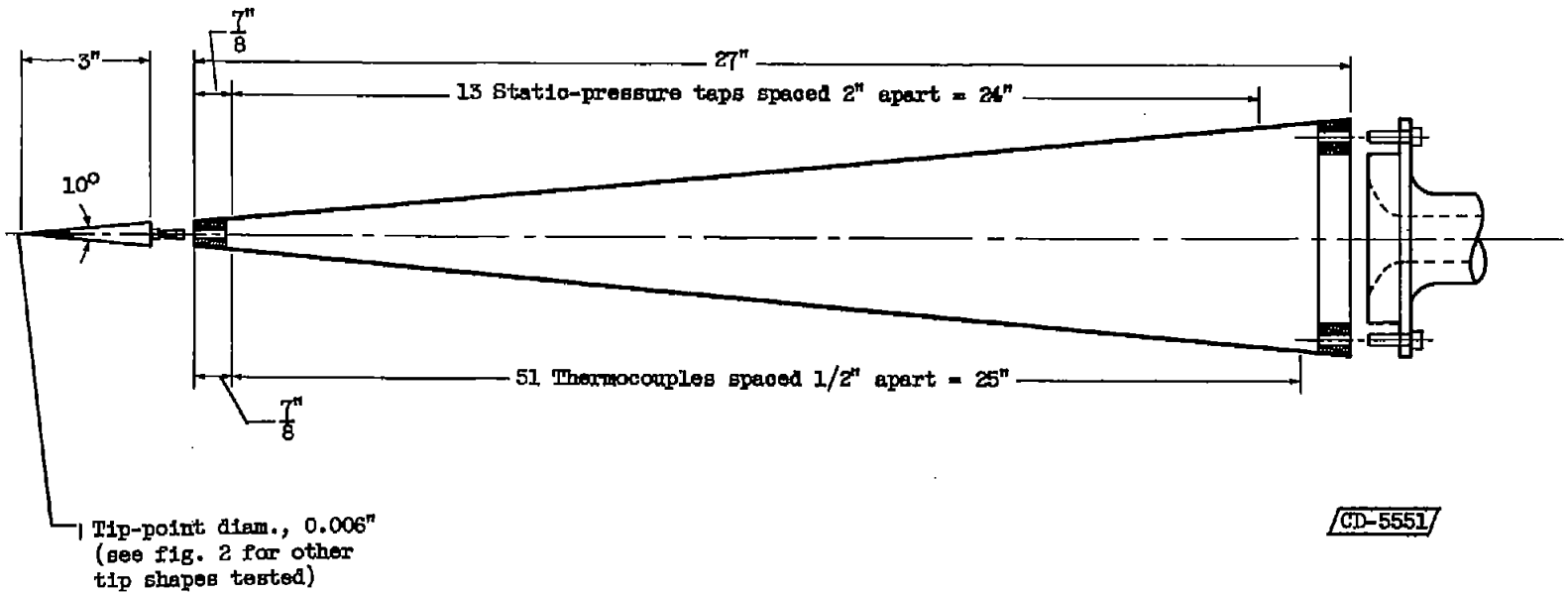

Figure 1. - Cone model used in investigation. Model shell, 0.032-inch-thick Inconel; surface-finish tolerance, ±8 microinches rms.

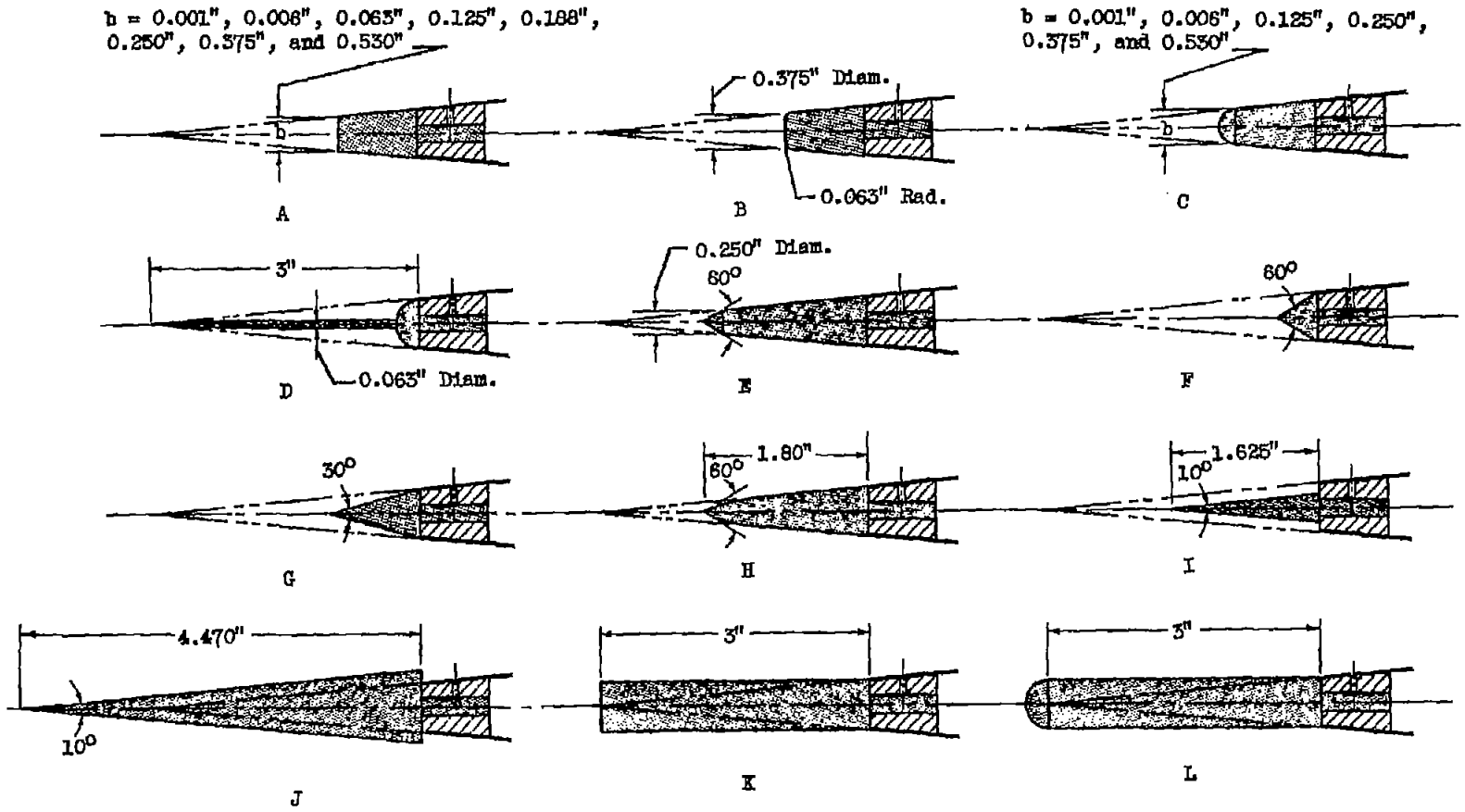

CD-5552

Figure 2. - Tip configurations used in investigation.

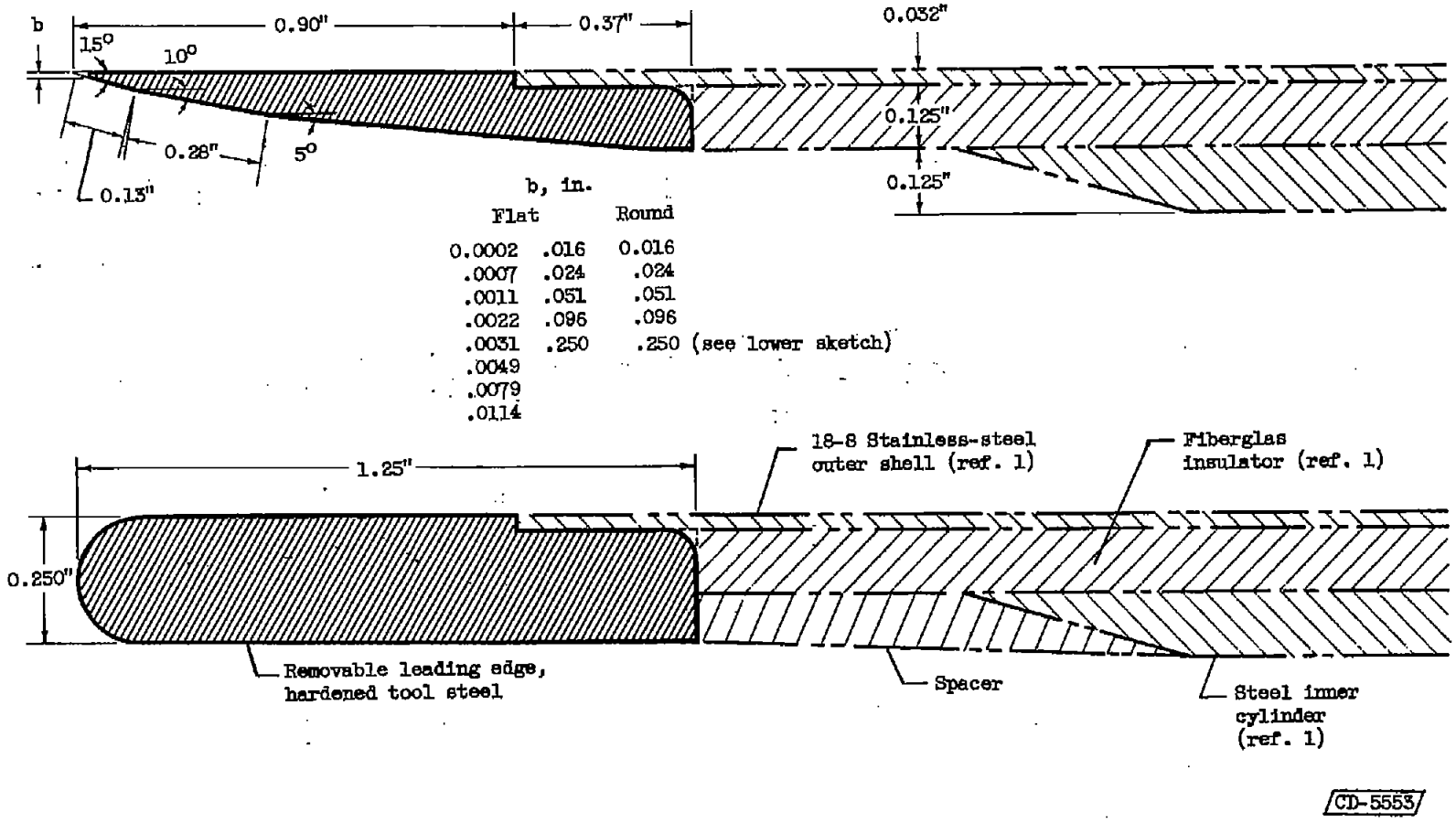

Figure 3. - Sections of cylinder bluntnesses investigated.

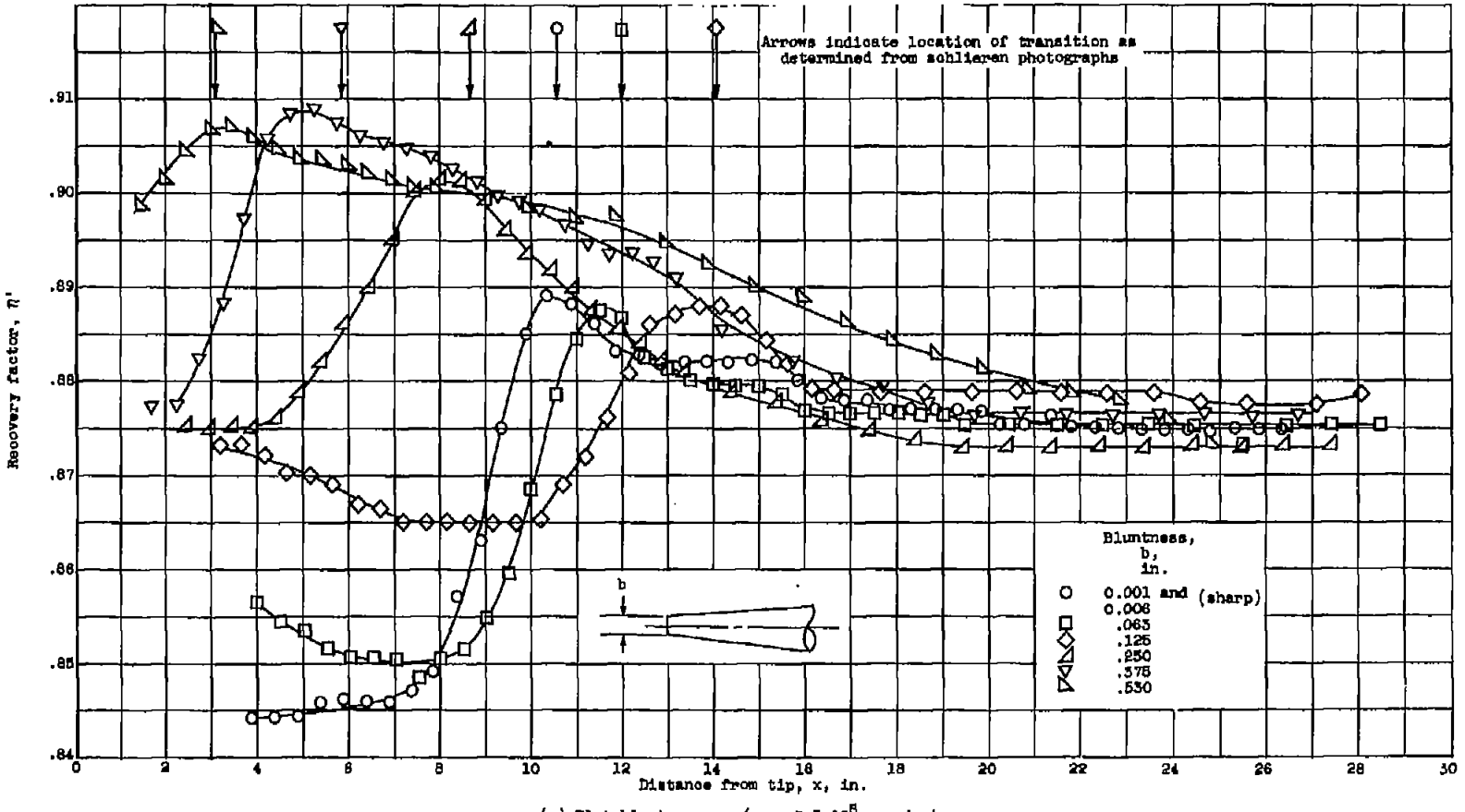

(a) Flat bluntness; $u_\infty/\nu_\infty = 3.5 \times 10^6$ per inch.

Figure 4. - Effect of cone bluntness on recovery-factor distribution and transition position.

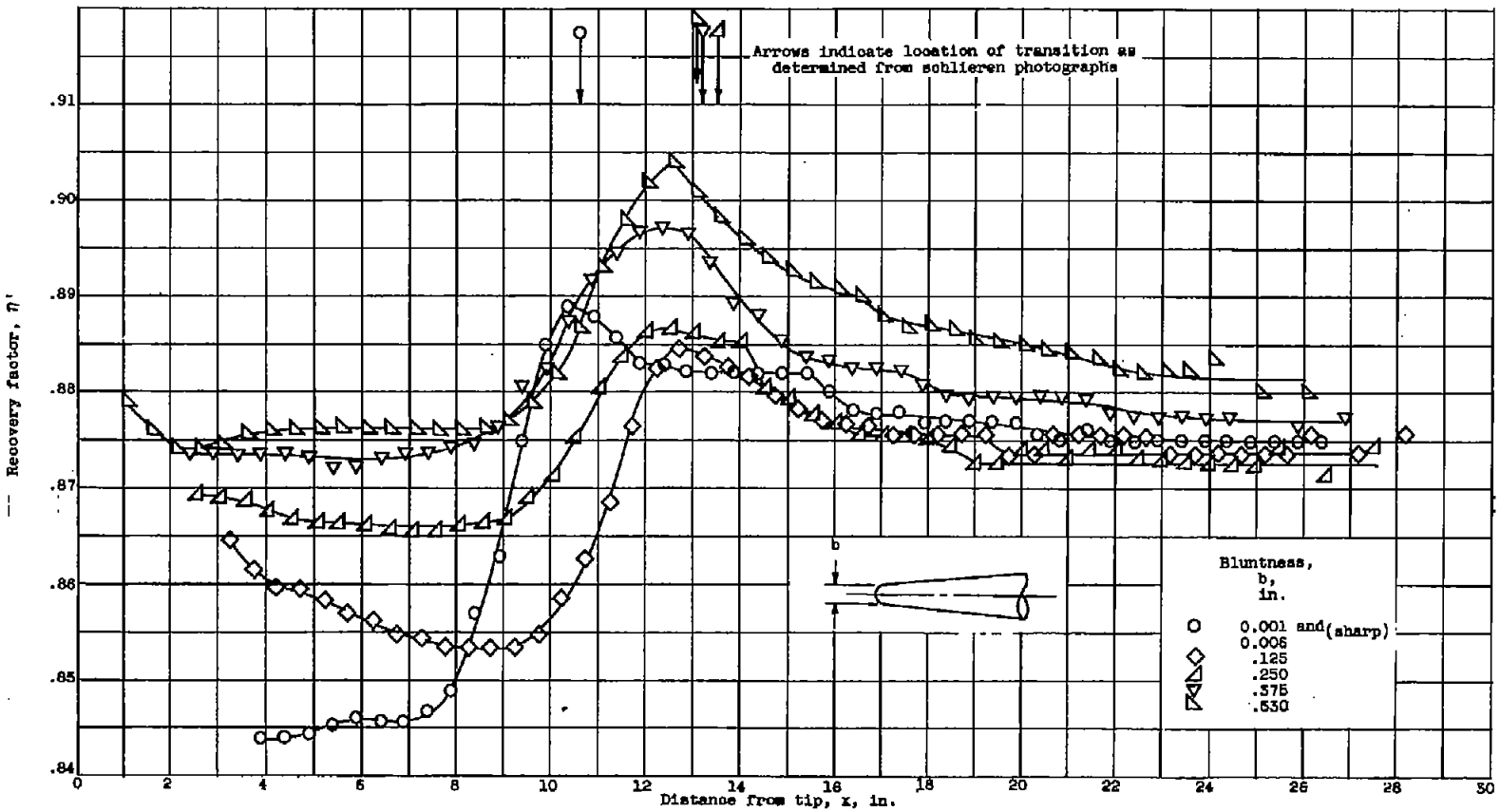

(b) Hemispherical bluntness; $u_\infty/\nu_\infty = 3.5\times10^5$ per inch.

Figure 4. - Concluded. Effect of cone bluntness on recovery-factor distribution and transition position.

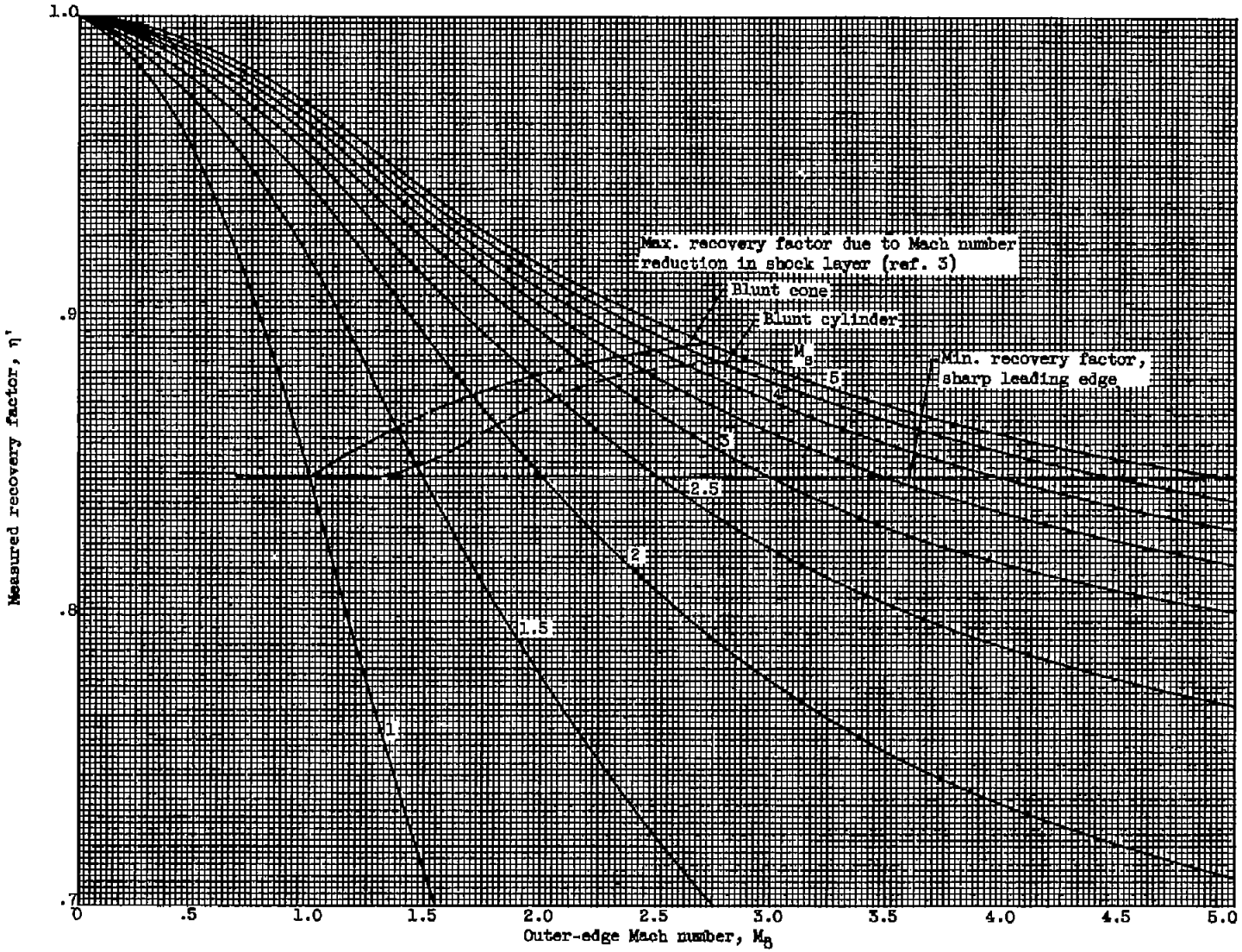

Figure 5. - Outer-edge Mach number computed from measured recovery factor.

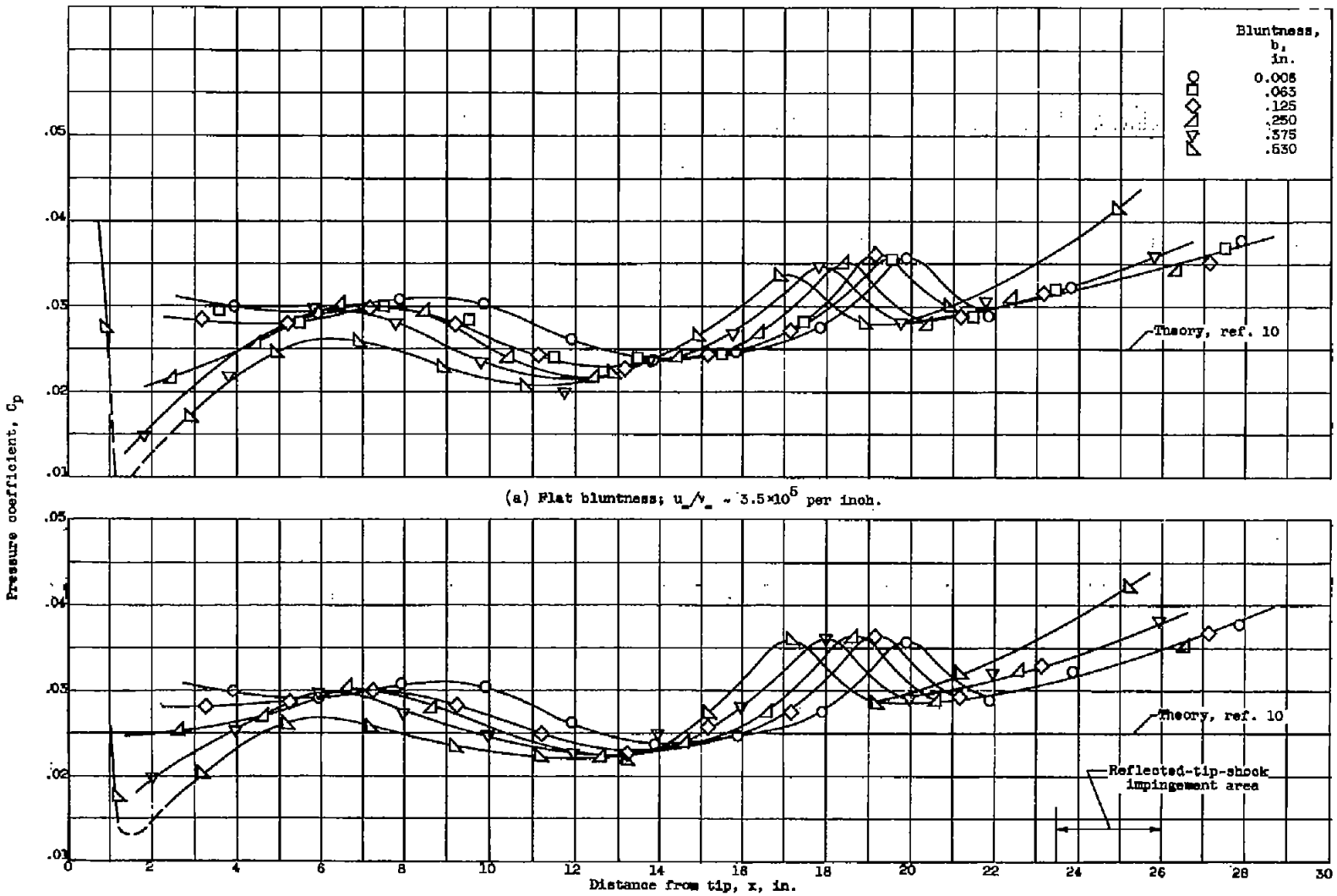

(a) Flat bluntness; $u_\infty/\nu_\infty \approx 3.5\times10^5$ per inch.

(b) Hemispherical bluntness; $u_\infty/\nu_\infty = 3.5\times10^5$ per inch.

Figure 8. - Effect of cone leading-edge bluntness on pressure distribution.

5046

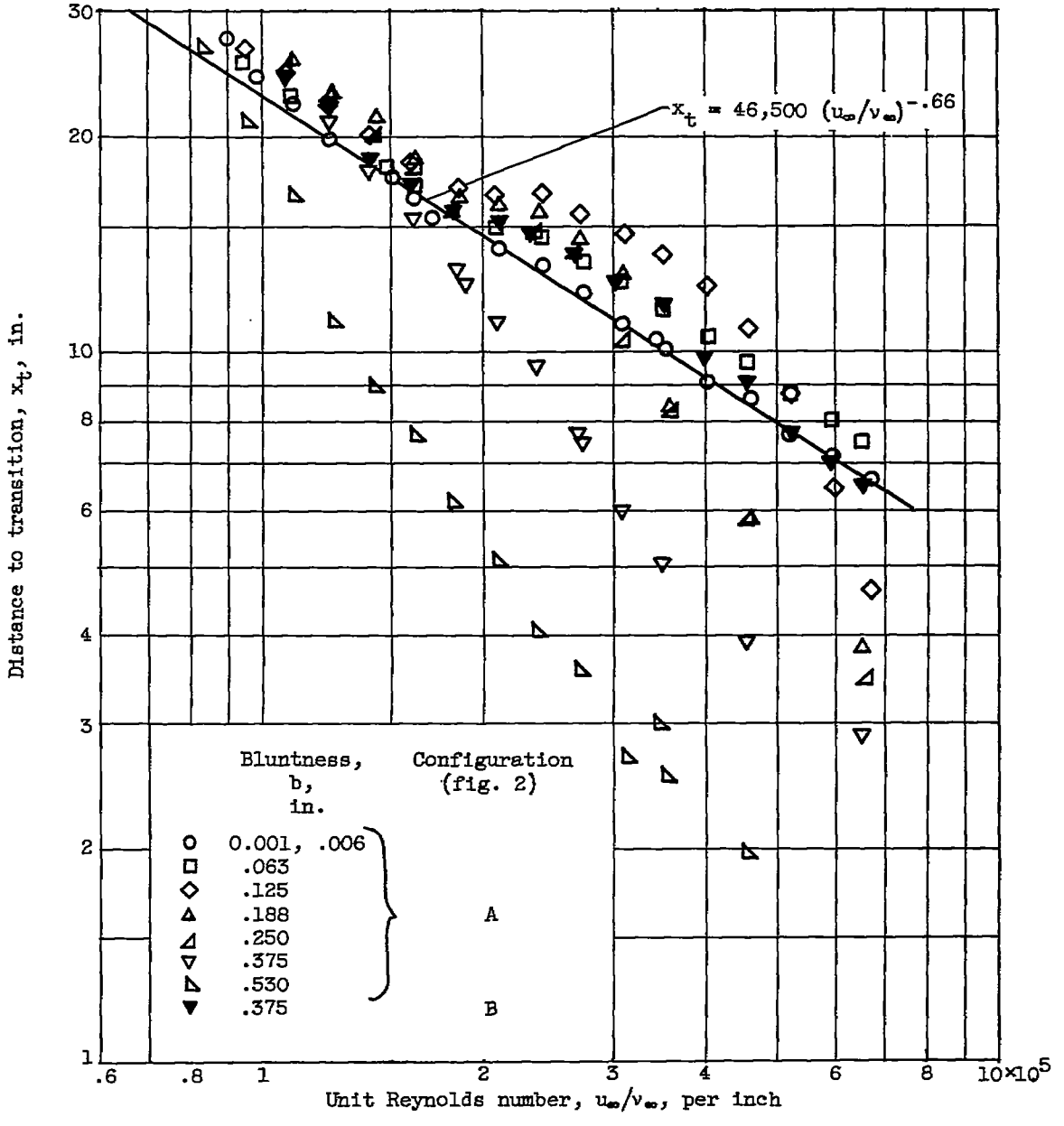

(a) Flat bluntness, configurations A and B.

Figure 7. - Effect of cone bluntness on distance to transition.

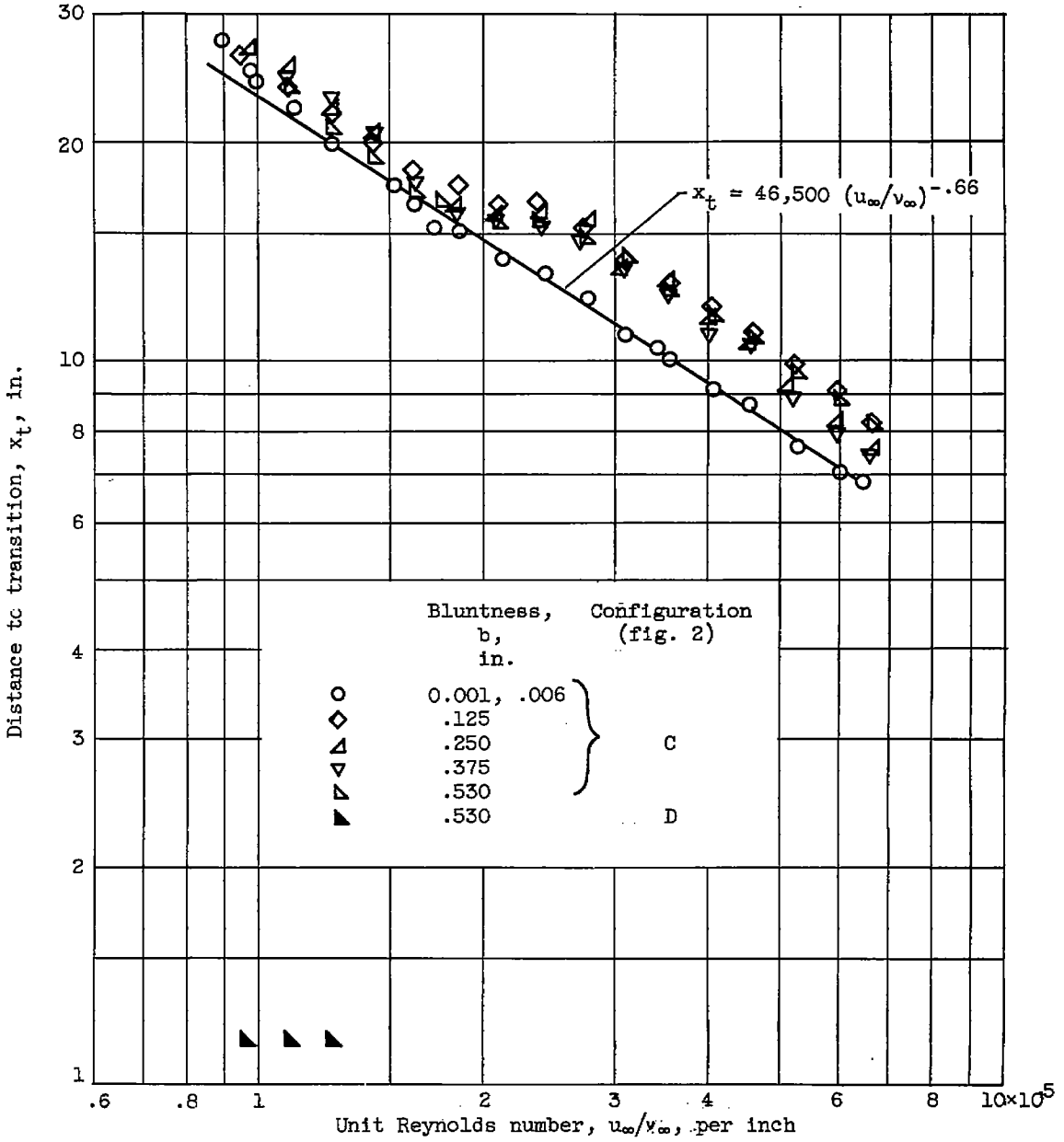

(b) Hemispherical bluntness, configurations C and D.

Figure 7. - Continued. Effect of cone bluntness on distance to transition.

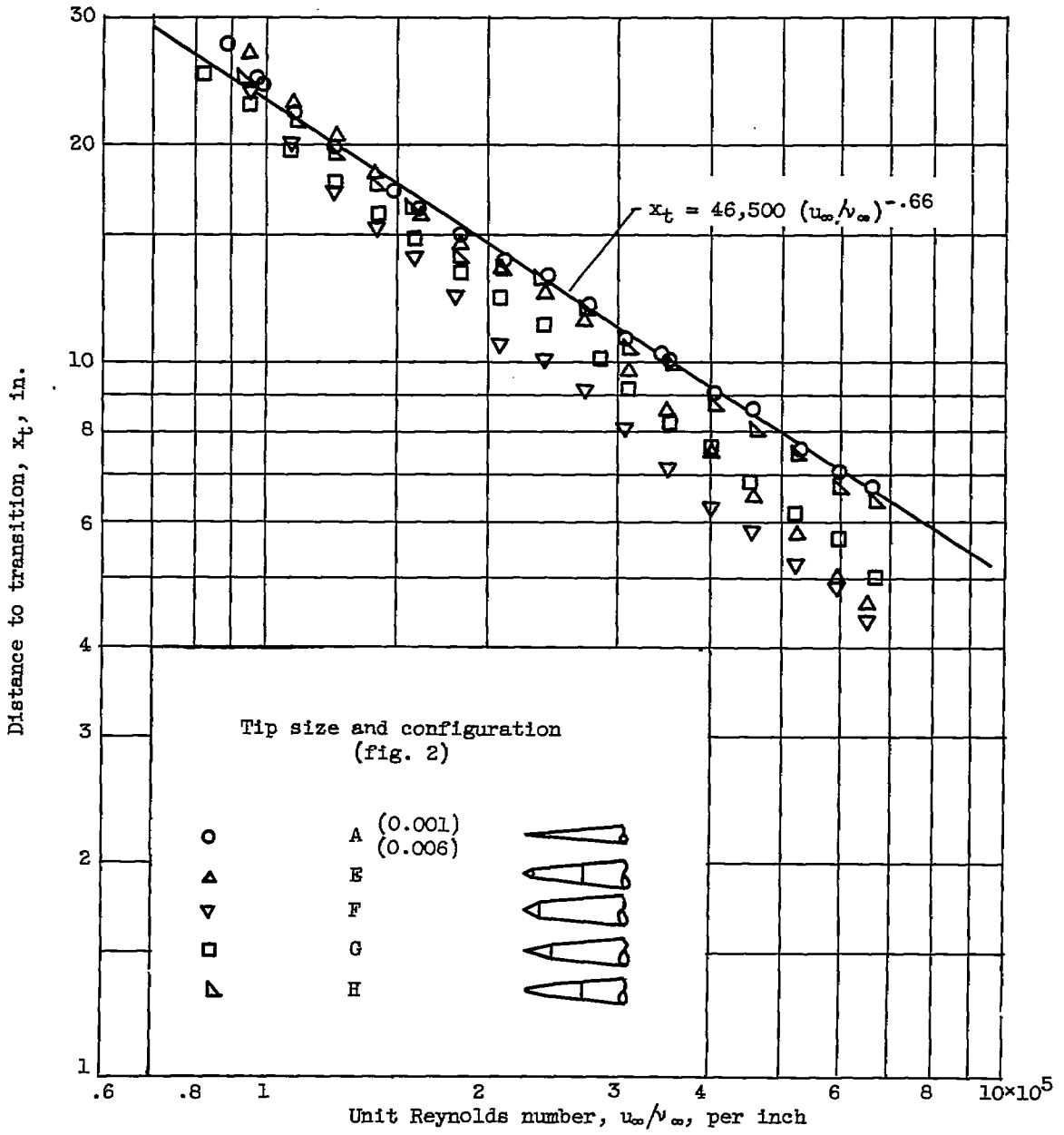

(c) Conical tips, configurations E to H.

Figure 7. - Continued. Effect of cone bluntness on distance to transition.

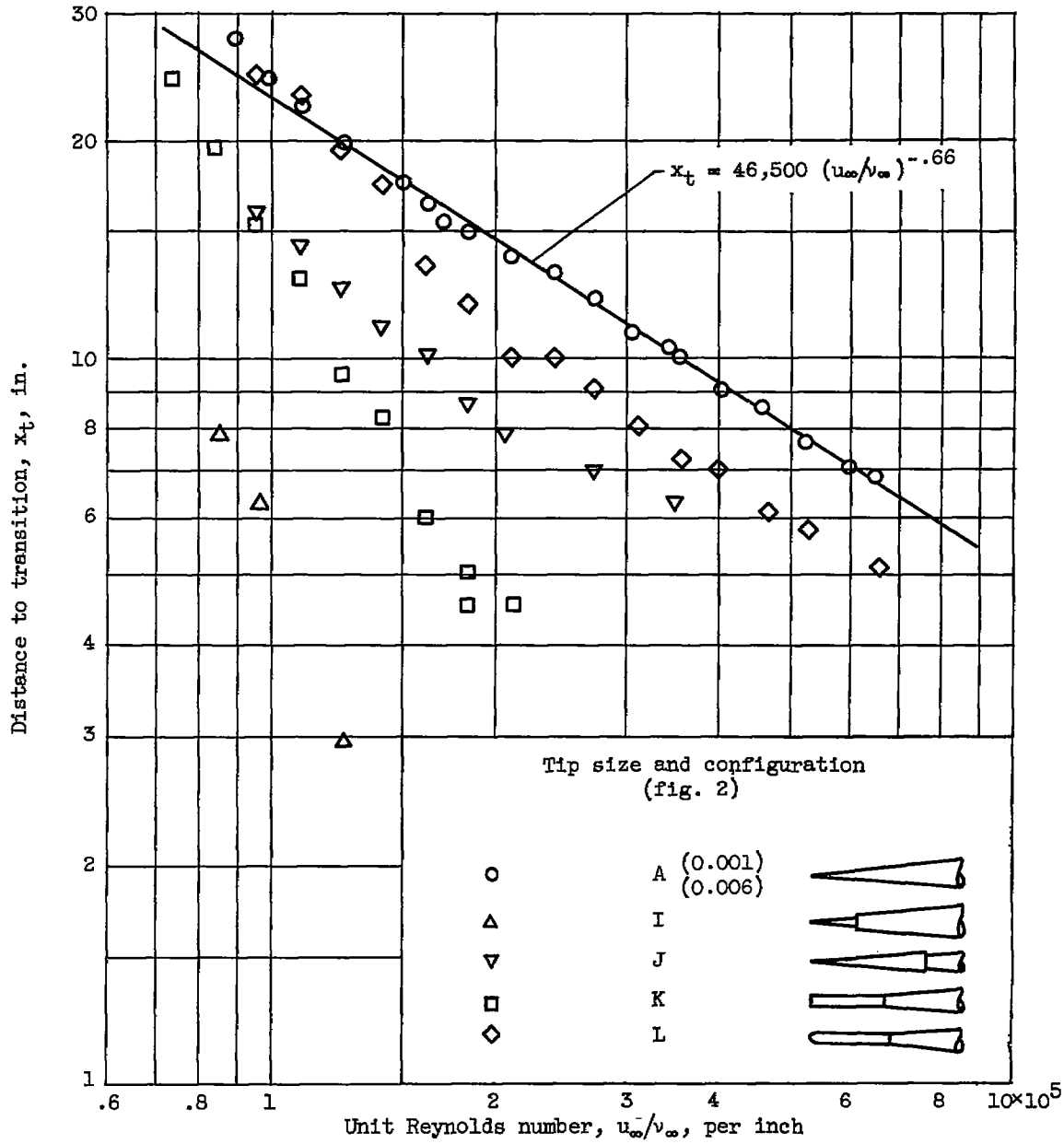

(d) Configurations I to K.

Figure 7. - Concluded. Effect of cone bluntness on distance to transition.

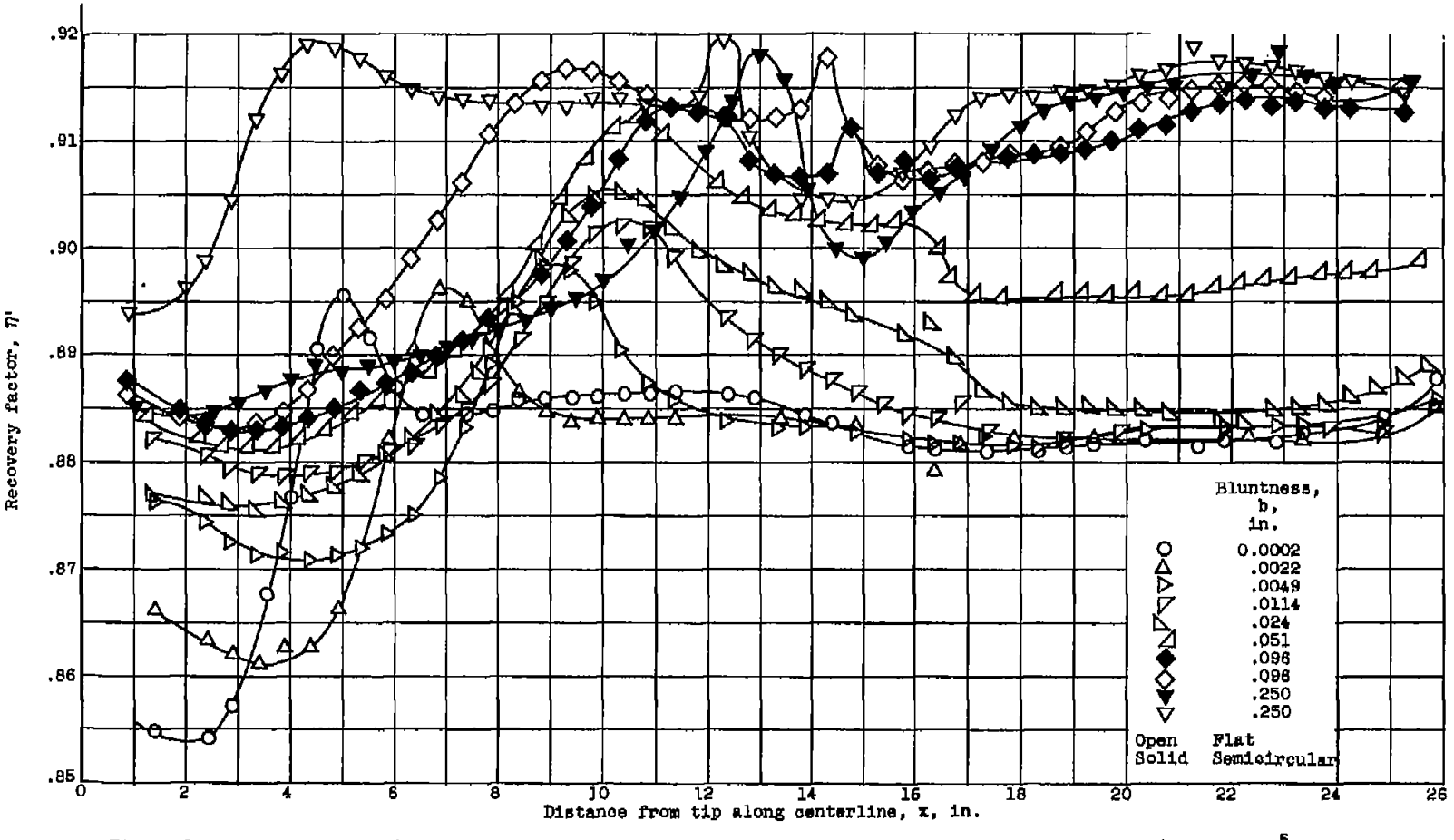

Figure 8. - Effect of cylinder bluntness on recovery-factor distribution and transition position; $u_\infty/\nu_\infty = 3.5\times10^5$ per inch.

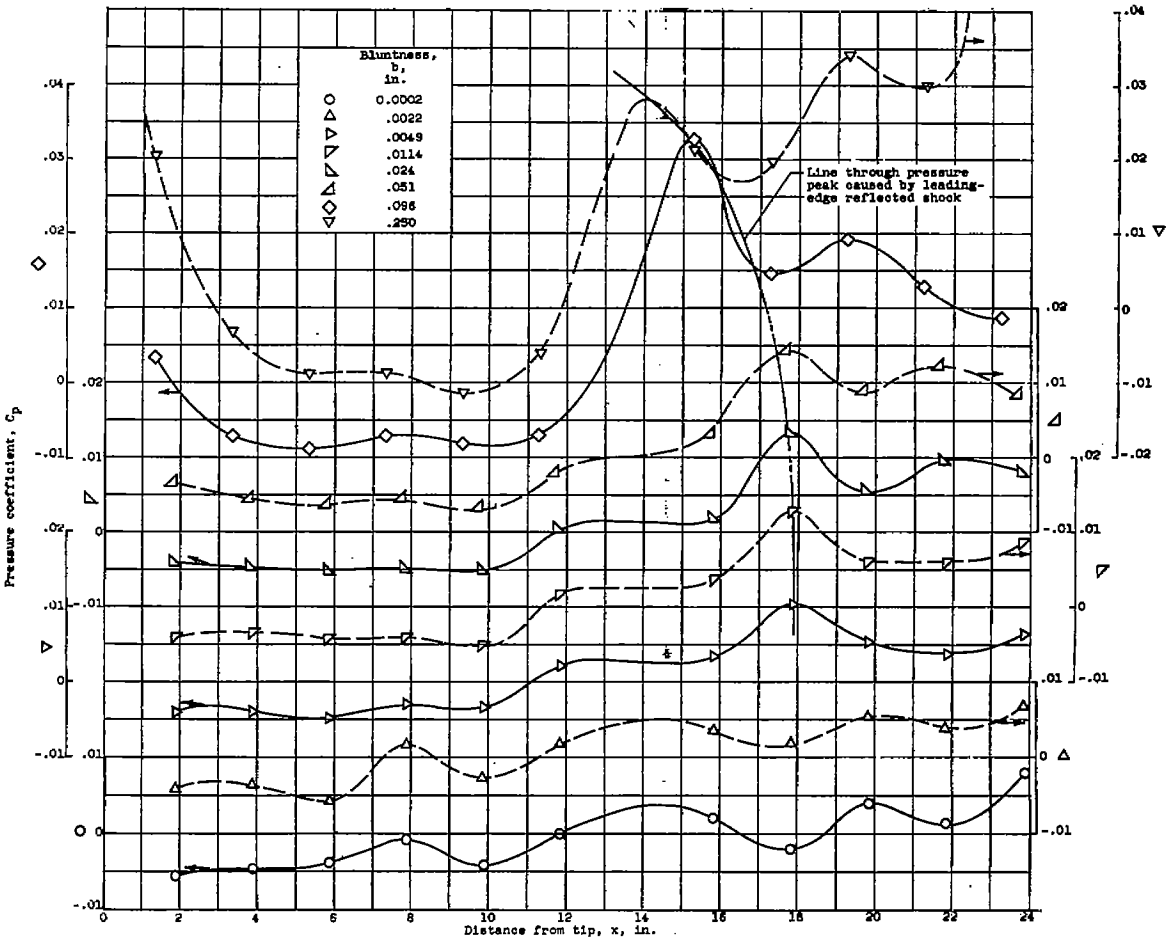

(a) Flat bluntness; $u_\infty/\nu_\infty = 3.5\times10^5$ per inch.

Figure 9. - Effect of cylinder leading-edge bluntness on pressure distribution.

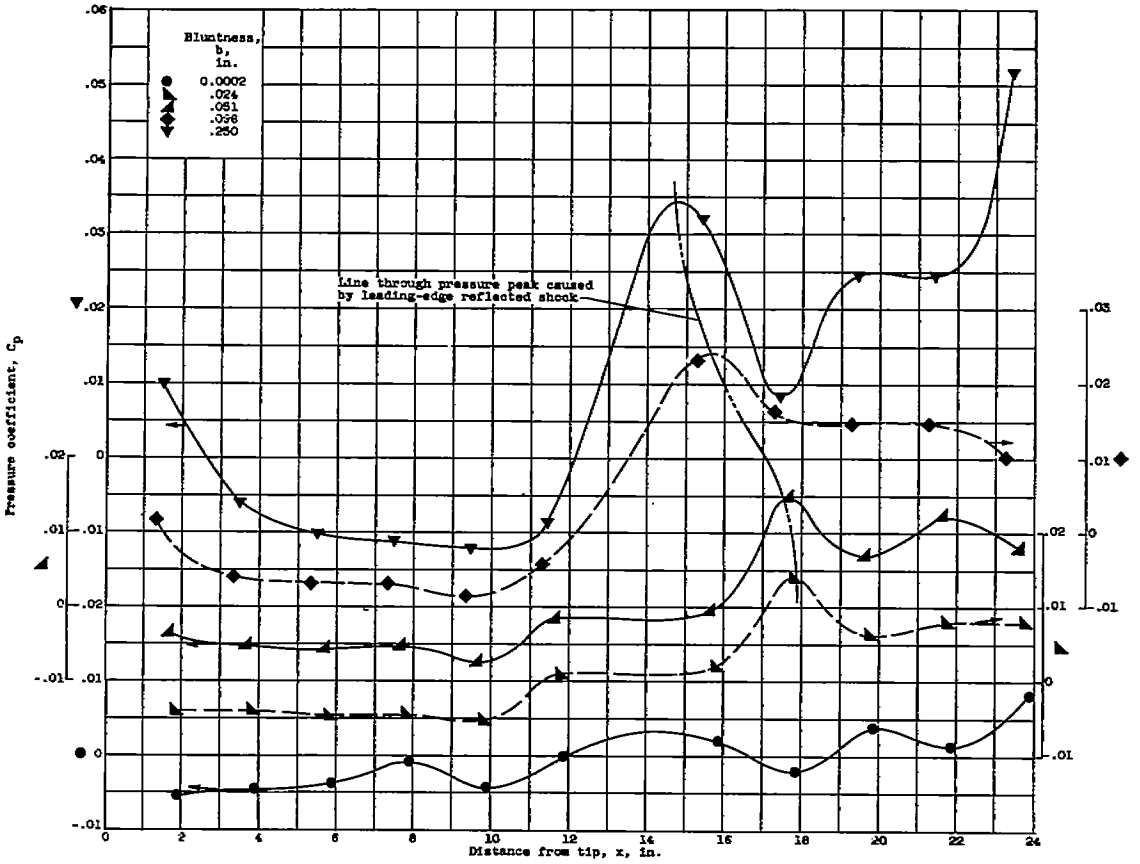

(b) Semicircular bluntness; $u_\infty/\nu_\infty = 3.5 \times 10^5$ per inch.

Figure 9. - Concluded. Effect of cylinder leading-edge bluntness on pressure distribution.

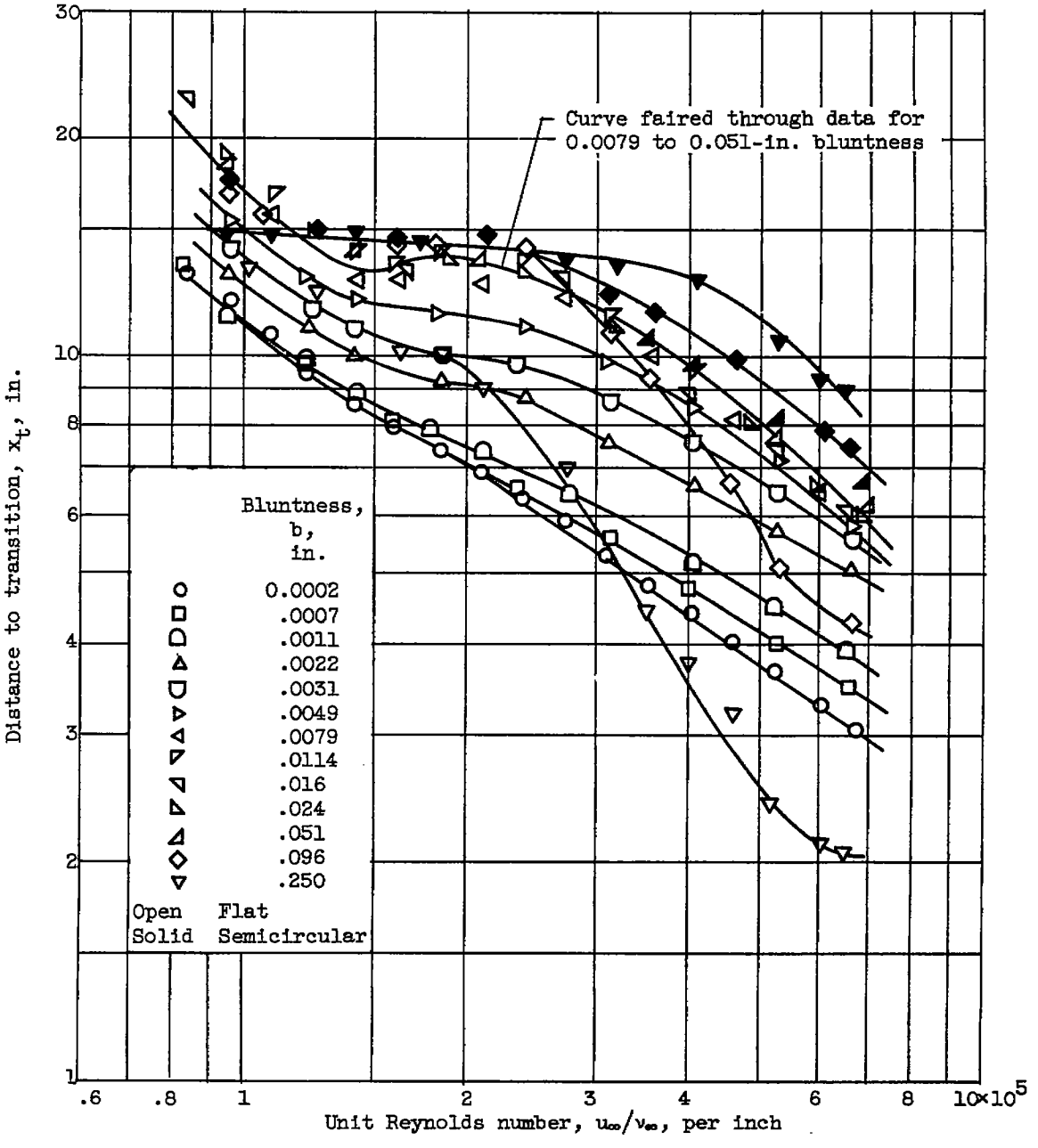

Figure 10. - Effect of bluntness on distance to transition for hollow cylinder.

5046

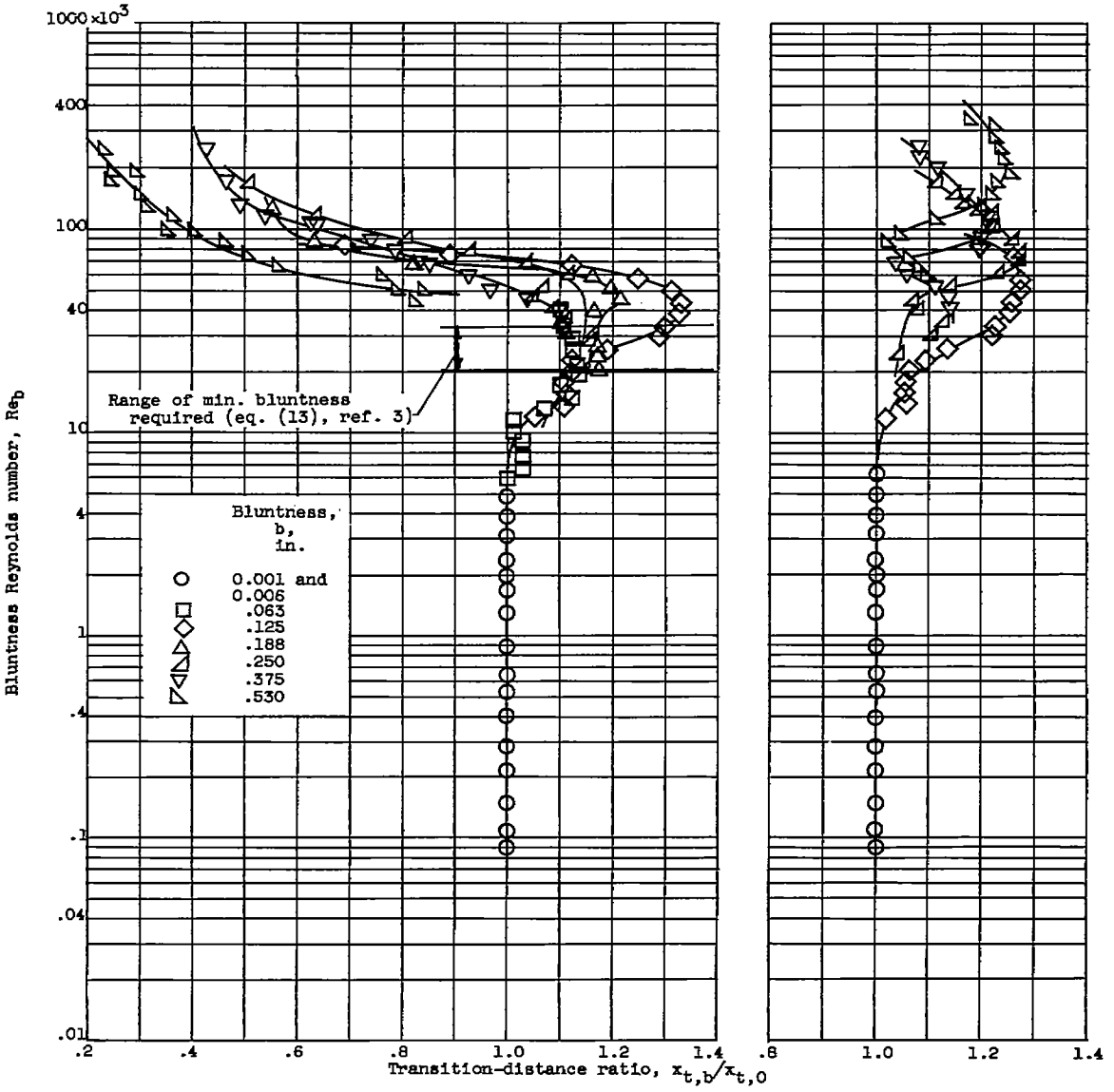

(a) Cone, flat bluntness. (b) Cone, hemispherical bluntness.

Figure 11. - Effect of cone and cylinder bluntness on transition-distance ratio.

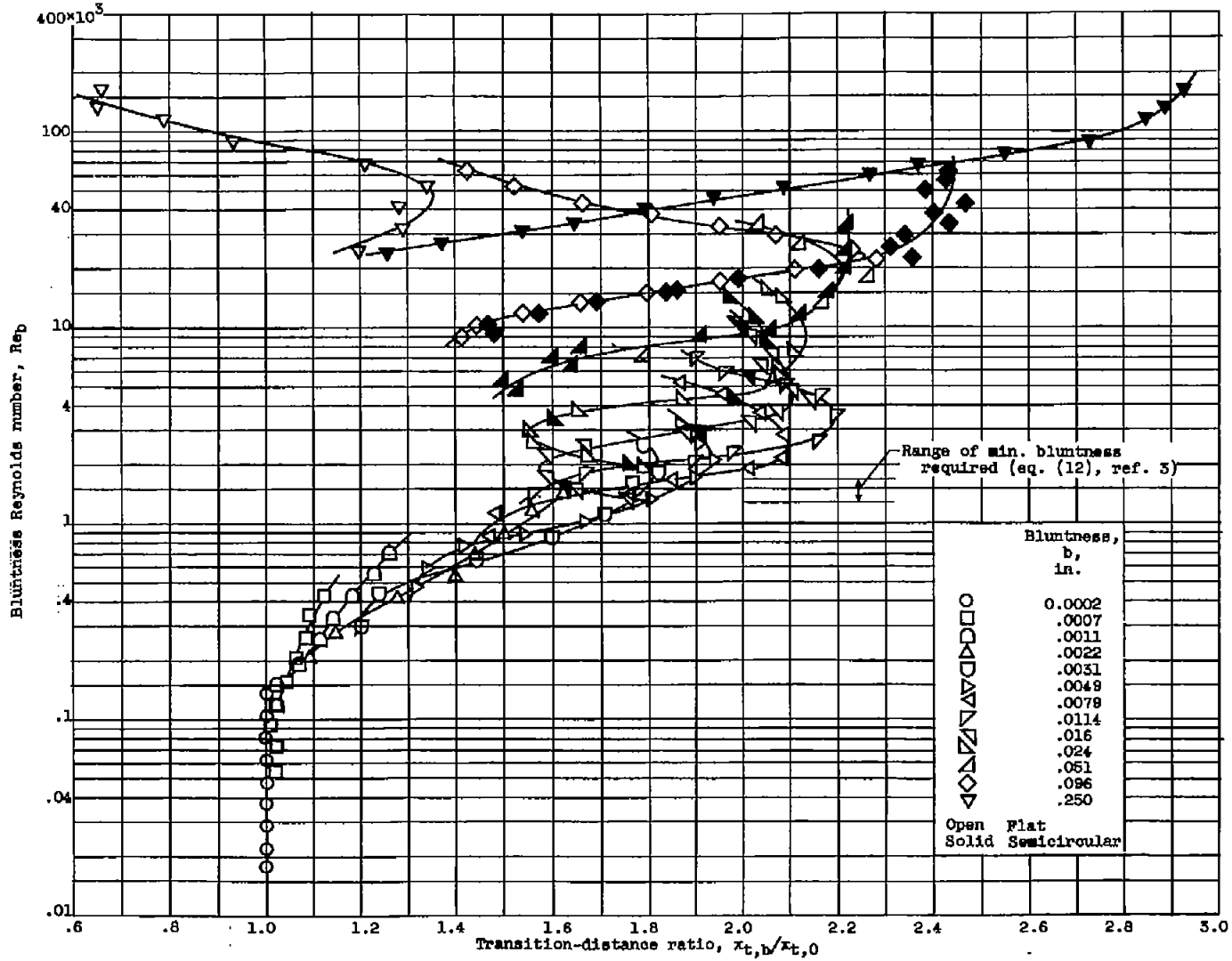

(c) Cylinder, flat and semicircular bluntness.

Figure 11. - Continued. Effect of cone and cylinder bluntness on transition-distance ratio.

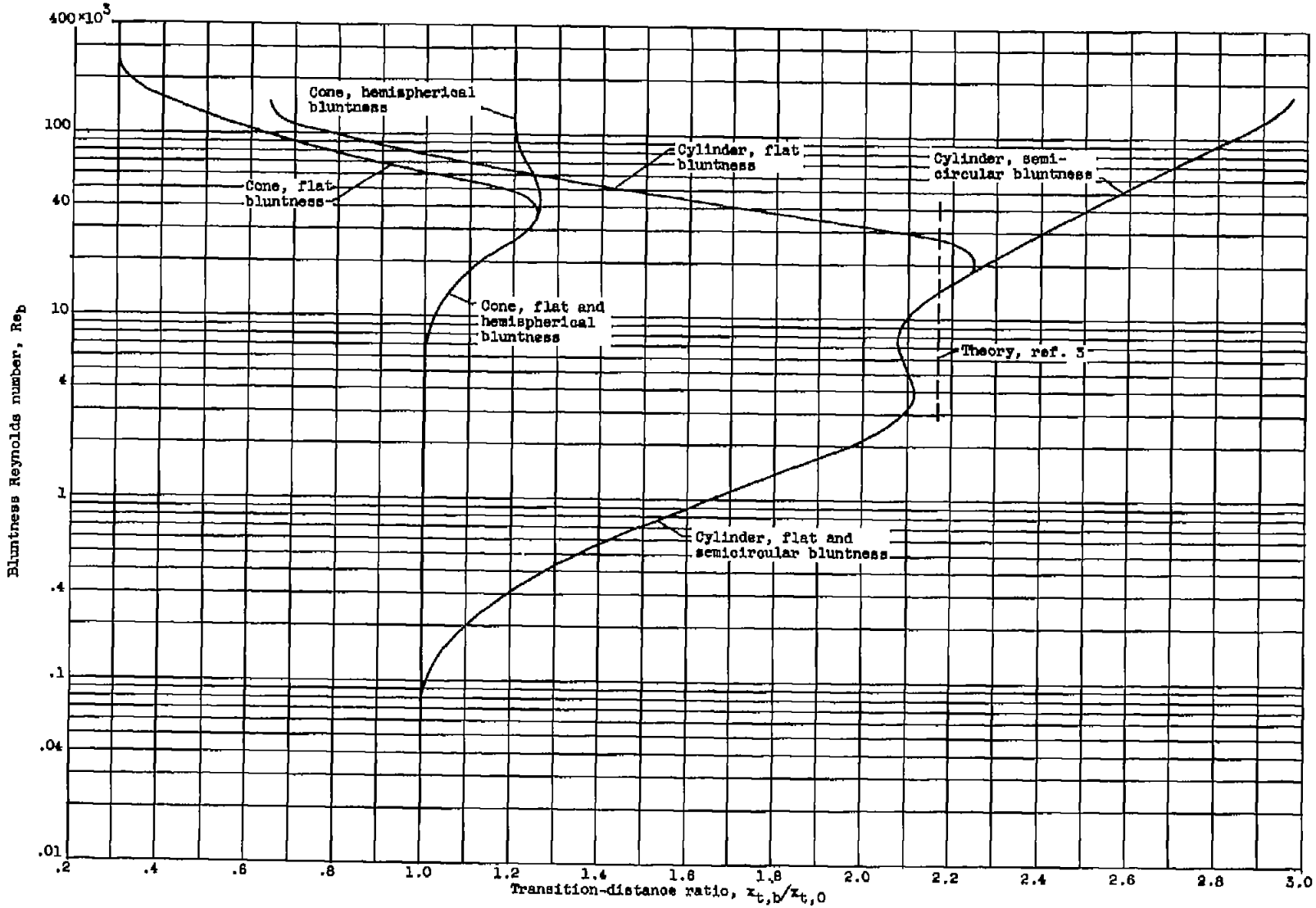

(d) Composite of figs. 11(a) to (c).

Figure 11. - Concluded. Effect of cone and cylinder bluntness on transition-distance ratio.

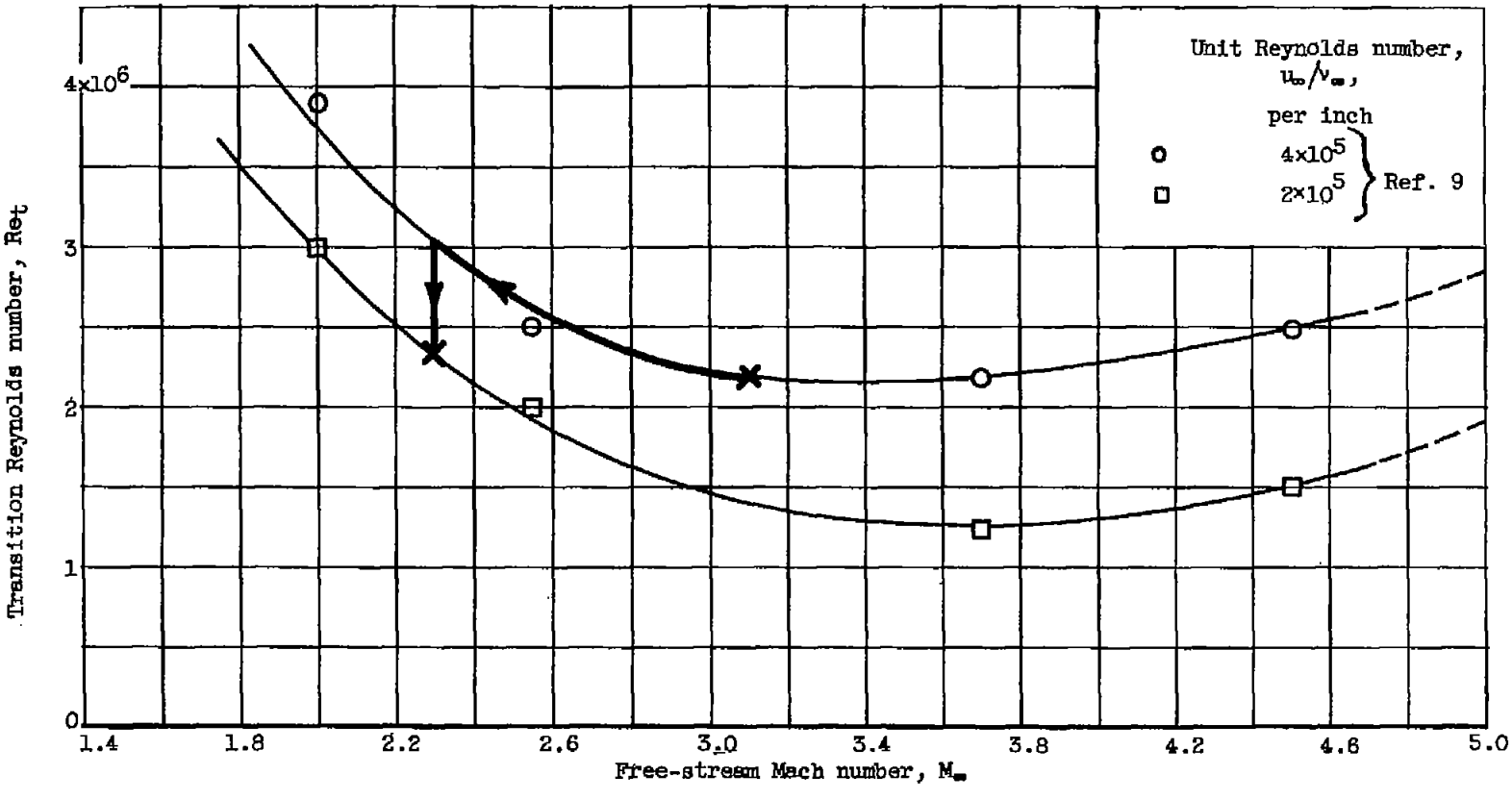

Figure 12. - Effect of Mach number reduction and unit Reynolds number reduction on transition Reynolds number.

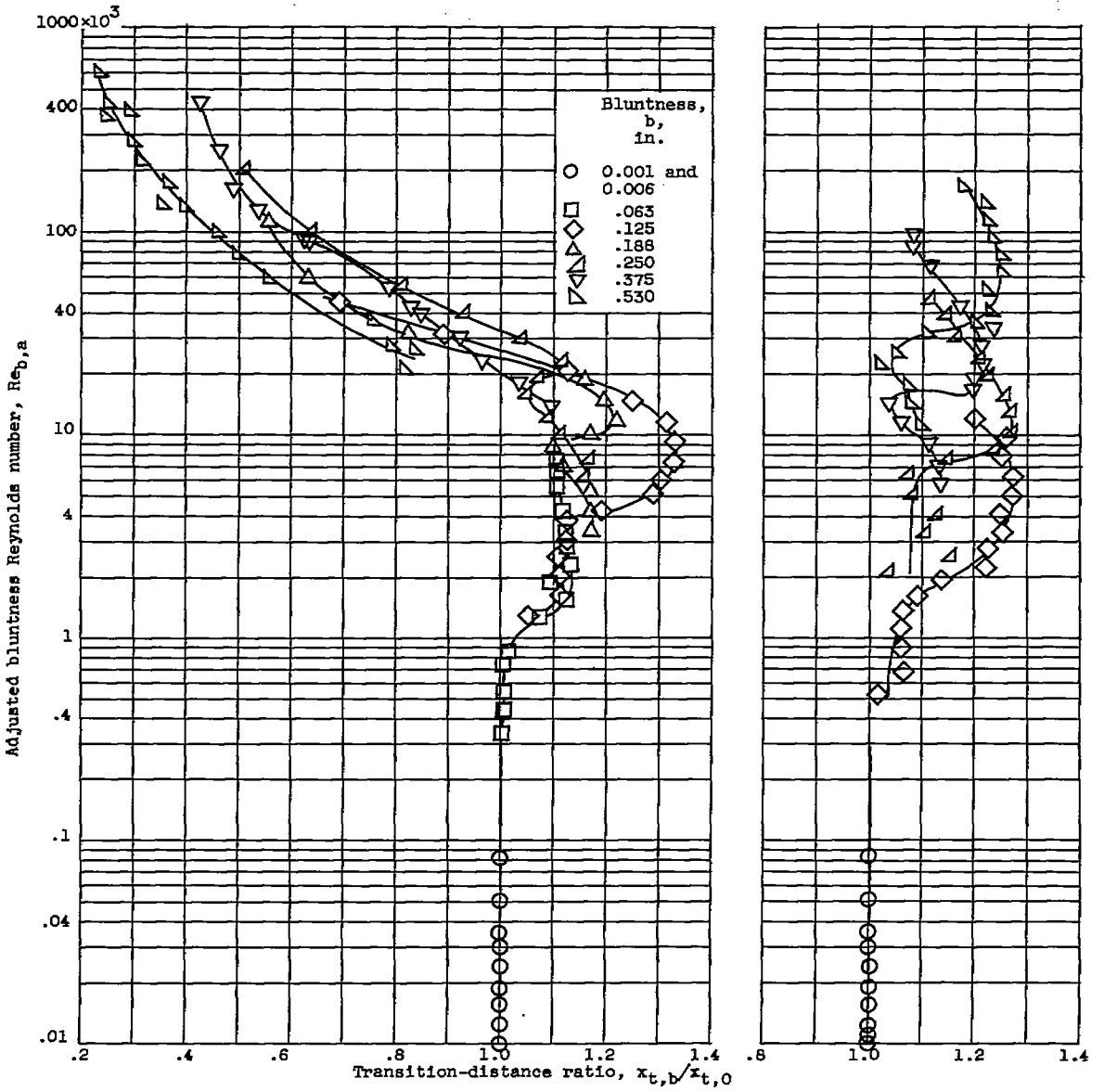

(a) Cone, flat bluntness. (b) Cone, hemispherical bluntness.

Figure 13. - Effect of cone and cylinder adjusted bluntness Reynolds number on transition-distance ratio.

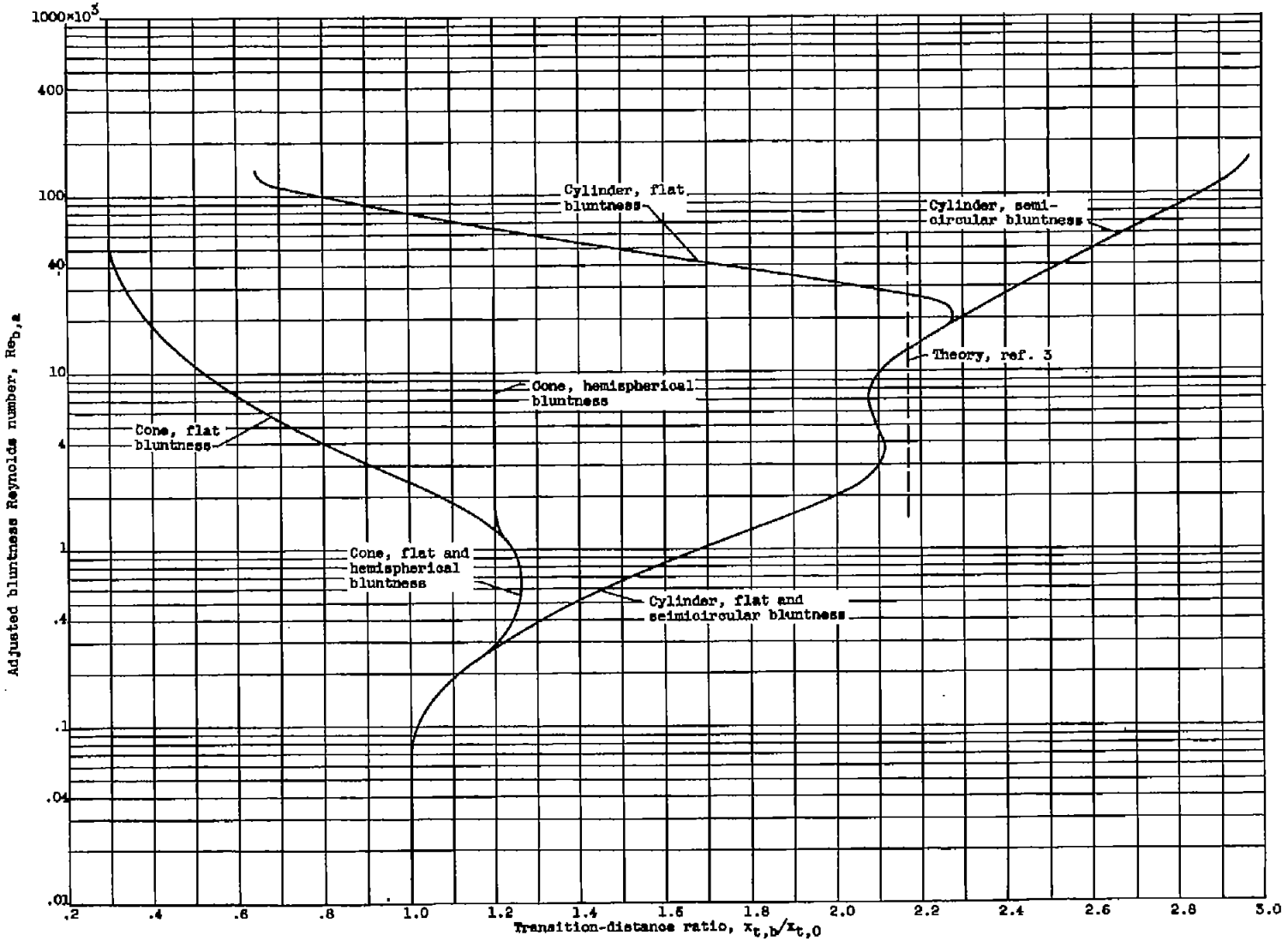

(a) Composite of figures 11(c) and 13(a) and (b).

Figure 13. - Concluded. Effect of cone and cylinder adjusted bluntness Reynolds number on transition-distance ratio.